Monthly Notices of the ROYAL ASTRONOMICAL SOCIETY

MNRAS **466,** 1242–1258 (2017) doi:10.1093/mnras/stw3090
Advance Access publication 2016 November 30

The CALYMHA survey: Lyα luminosity function and global escape fraction of Lyα photons at $z = 2.23$

David Sobral,[1,2★] Jorryt Matthee,[2★] Philip Best,[3] Andra Stroe,[4†] Huub Röttgering,[2] Iván Oteo,[3,4] Ian Smail,[5] Leah Morabito[2] and Ana Paulino-Afonso[6,7]

[1] *Department of Physics, Lancaster University, Lancaster LA1 4YB, UK*
[2] *Leiden Observatory, Leiden University, PO Box 9513, NL-2300 RA Leiden, the Netherlands*
[3] *Institute for Astronomy, University of Edinburgh, Royal Observatory, Blackford Hill, Edinburgh EH9 3HJ, UK*
[4] *European Southern Observatory, Karl-Schwarzschild-Str. 2, D-85748 Garching, Germany*
[5] *Centre for Extragalactic Astronomy, Department of Physics, Durham University, South Road, Durham DH1 3LE, UK*
[6] *Instituto de Astrofísica e Ciências do Espaço, Universidade de Lisboa, OAL, Tapada da Ajuda, P-1349-018 Lisbon, Portugal*
[7] *Departamento de Física, Faculdade de Ciências, Universidade de Lisboa, Campo Grande, P-1749-016 Lisbon, Portugal*

Accepted 2016 November 25. Received 2016 November 25; in original form 2016 July 25

ABSTRACT

We present the CAlibrating LYMan-α with Hα (CALYMHA) pilot survey and new results on Lyman α (Lyα) selected galaxies at $z \sim 2$. We use a custom-built Lyα narrow-band filter at the Isaac Newton Telescope, designed to provide a matched volume coverage to the $z = 2.23$ Hα HiZELS survey. Here, we present the first results for the COSMOS and UDS fields. Our survey currently reaches a 3σ line flux limit of $\sim 4 \times 10^{-17}$ erg s^{-1} cm^{-2}, and a Lyα luminosity limit of $\sim 10^{42.3}$ erg s^{-1}. We find 188 Lyα emitters over 7.3×10^5 Mpc^3, but also find significant numbers of other line-emitting sources corresponding to He II, C III] and C IV emission lines. These sources are important contaminants, and we carefully remove them, unlike most previous studies. We find that the Lyα luminosity function at $z = 2.23$ is very well described by a Schechter function up to $L_{\mathrm{Ly}\alpha} \approx 10^{43}$ erg s^{-1} with $L^* = 10^{42.59^{+0.16}_{-0.08}}$ erg s^{-1}, $\phi^* = 10^{-3.09^{+0.14}_{-0.34}}$ Mpc^{-3} and $\alpha = -1.75 \pm 0.25$. Above $L_{\mathrm{Ly}\alpha} \approx 10^{43}$ erg s^{-1}, the Lyα luminosity function becomes power-law like, driven by X-ray AGN. We find that Lyα-selected emitters have a high escape fraction of 37 ± 7 per cent, anticorrelated with Lyα luminosity and correlated with Lyα equivalent width. Lyα emitters have ubiquitous large ($\approx$40 kpc) Lyα haloes, $\sim$2 times larger than their Hα extents. By directly comparing our Lyα and Hα luminosity functions, we find that the global/overall escape fraction of Lyα photons (within a 13 kpc radius) from the full population of star-forming galaxies is 5.1 ± 0.2 per cent at the peak of the star formation history. An extra 3.3 ± 0.3 per cent of Lyα photons likely still escape, but at larger radii.

Key words: galaxies: evolution – galaxies: haloes – galaxies: high-redshift – galaxies: luminosity function, mass function – galaxies: statistics – cosmology: observations.

1 INTRODUCTION

Understanding galaxy formation and evolution requires significant efforts on both theoretical and observational sides. Observations show that the star formation activity in the Universe was over 10 times higher in the past, reaching a peak at $z \sim 2$–3 (e.g. Lilly et al. 1996; Karim et al. 2011; Sobral et al. 2013). Most of this increase is explained by typical star formation rates (SFRs) of galaxies at $z \sim 2$ being a factor of $\sim$10 times higher than at $z = 0$ (e.g. Smit et al. 2012; Sobral et al. 2014; Stroe & Sobral 2015), likely driven, to first order, by relatively high gas fractions (e.g. Tacconi et al. 2010; Saintonge et al. 2011; Stott et al. 2016). Beyond $z \sim 2$–3, UV and rest-frame optical emission line studies suggest a decline of the star formation history of the Universe with increasing redshift (e.g. Bouwens et al. 2015; Khostovan et al. 2015).

While the UV is the main way of photometrically selecting $z > 3$ star-forming galaxies, by taking advantage of the Lyman-break technique (e.g. Steidel et al. 1996; Giavalisco 2002), the Lyman α (Lyα) emission line is by far the most used for spectroscopically confirming and studying very distant galaxies (e.g. Ono et al. 2012; Oesch et al. 2015; Sobral et al. 2015b; Zitrin et al. 2015). Lyα has also been widely used to obtain large samples of galaxies through

★ E-mail: d.sobral@lancaster.ac.uk (DS); matthee@strw.leidenuniv.nl (JM)
† ESO Fellow.

the narrow-band selection (e.g. Ouchi et al. 2008, 2010; Matthee et al. 2015; Santos, Sobral & Matthee 2016) and to find distant galaxies with extremely young and likely metal-poor stellar populations (e.g. Kashikawa et al. 2012; Sobral et al. 2015b). The Lyα line is also used to study the interstellar (e.g. Swinbank et al. 2015), circumgalactic and/or intergalactic medium (e.g. Sargent et al. 1980; Hernquist et al. 1996). This is facilitated by the fact that Lyα emission line is intrinsically the brightest emission line in H II regions (e.g. Partridge & Peebles 1967; Pritchet 1994), and due to the fact that it is redshifted into easily observed optical wavelengths beyond $z \sim 2$ (see also Dijkstra 2014).

The Lyα luminosity function has been found to evolve very strongly from $z \sim 0$ to $\sim$3 for relatively faint Lyα emitters (e.g. Ouchi et al. 2008; Cowie, Barger & Hu 2010; Barger, Cowie & Wold 2012; Drake et al. 2016). At $z \sim 2$, the Lyα luminosity function has been studied by e.g. Hayes et al. (2010) and Konno et al. (2016), with significant disagreements probably explained by the expected strong cosmic variance (see Sobral et al. 2015a). Konno et al. (2016) also finds a significant deviation from a Schechter function for $L_{\mathrm{Ly}\alpha} > L^*$, consistent with results seen for Hα-selected samples from Sobral et al. (2016). However, an important issue that needs to be addressed is the contamination by other lines. Most Lyα surveys assume that contaminants are negligible (e.g. Konno et al. 2016), but that is not necessarily the case (e.g. Matthee et al. 2015; Nakajima et al. 2016; Santos et al. 2016).

Despite much progress in selecting Lyα emitters through large surveys, the nature and evolution of Lyα sources are still a matter of debate. For example, recent advances with IFU surveys using the MUSE instrument on the VLT (e.g. Bacon et al. 2015; Karman et al. 2015) confirm a population of Lyα emitters at $z \sim 3$–6 which are completely undetected in the deepest broad-band photometric surveys, due to their very high equivalent widths (EWs). Hundreds of similar candidate Lyα emitters were previously discovered by e.g. the Subaru telescope (Malhotra & Rhoads 2004; Kashikawa et al. 2006; Murayama et al. 2007; Ouchi et al. 2008, 2010). This is consistent with many Lyα emitters at $z > 3$ being typically low mass, blue and likely low metallicity (e.g. Gawiser et al. 2007; Gronwall et al. 2007; Ono et al. 2010b; Sobral et al. 2015b; Nakajima et al. 2016). However, studies closer to the peak of star formation history at $z \sim 2$ reveal Lyα sources which differ from those typical characteristics (e.g. Stiavelli et al. 2001; Bongiovanni et al. 2010; Oteo et al. 2015; Hathi et al. 2016). Some are found to be relatively massive, dusty (e.g. Chapman et al. 2005; Matthee et al. 2016b) and red (e.g. Stiavelli et al. 2001; Oteo et al. 2012a, 2015; Sandberg et al. 2015). Below $z \sim 3$, studies find that luminous Lyα emitters are progressively AGN dominated and more evolved (Nilsson et al. 2009; Cowie et al. 2010; Barger et al. 2012; Wold, Barger & Cowie 2014), although others can easily be considered analogues of $z > 3$ emitters (e.g. Barger et al. 2012; Oteo et al. 2012b; Erb et al. 2016; Trainor et al. 2016).

Many of the key limitations/questions about Lyα emitters result directly from Lyα's complex radiative transfer (e.g. Verhamme, Schaerer & Maselli 2006; Dijkstra, Lidz & Wyithe 2007; Verhamme et al. 2008; Gronke, Bull & Dijkstra 2015; Gronke & Dijkstra 2016). The resonant nature of the Lyα line results in Lyα photons scattering in neutral hydrogen, substantially increasing the likelihood of absorption by interstellar dust (e.g. Atek et al. 2008; Hayes 2015). Thus, Lyα luminosity can be significantly reduced, or even completely suppressed (e.g. Verhamme et al. 2008; Atek et al. 2009; Hayes et al. 2011; Atek et al. 2014). Theoretical galaxy formation models predict $f_{\mathrm{esc}} = 2$–10 per cent (e.g. Le Delliou et al. 2006; Nagamine et al. 2010; Garel et al. 2015) at $z = 2$–3, but are limited

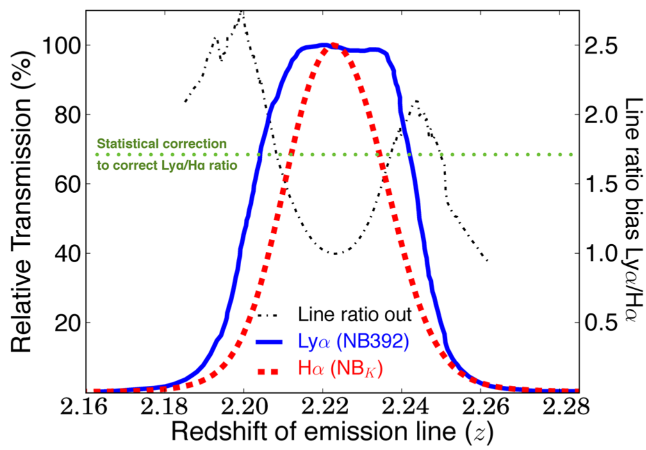

Figure 1. The transmission curves of our NB392 filter, primarily targeting the Lyα emission line at $z = 2.23$, and our NB$_K$ filter (Sobral et al. 2013), which targets Hα at the same redshift. We also show how observed line ratios vary as a function of redshift on a source by source basis, while we show the global correction for statistical samples that are randomly distributed in redshift. Note that the most significant biases are found in the wings, but the probability of finding a source, within a statistical sample, in the wings, is extremely low.

by a large number of assumptions which only direct observations can verify. Furthermore, a major limitation for models is the need for a compromise between the resolution required for radiative transfer and the need to simulate large enough volumes to be representative. For Lyα-selected samples (biased towards high Lyα escape fractions) at $z \sim 2$–3 (e.g. Nilsson et al. 2009), the comparison of Lyα with the UV suggests Lyα escape fractions, f_{esc}, of 30–60 per cent (e.g. Wardlow et al. 2014; Trainor et al. 2015).

One way to improve our understanding of Lyα-selected sources and its escape fraction is the comparison with a well understood, non-resonant recombination emission line, such as Hα. Hayes et al. (2010) provided such a study for a relatively small volume at $z = 2.2$, finding a global $\sim$5 per cent escape fraction. More recently, Matthee et al. (2016b) studied a sample of $\sim$1000 Hα-selected galaxies, to find that the Lyα escape fraction strongly depends on the aperture used and on SFR. Konno et al. (2016) have also presented a statistical global escape fraction measurement by comparing their Lyα luminosity function with the UV or with the Hα luminosity function from Sobral et al. (2013). Sandberg et al. (2015) presented an Hα–Lyα study over the GOODS N field at $z \sim 2$, but the small sample size and the typical low luminosity of the sources greatly limits their conclusions. A significant advance can only be obtained with a panoramic survey, covering the full range of environments, and having access to both Lyα and Hα.

In order to address current shortcomings, we are carrying out the CALYMHA survey: CAlibrating LYMan-α with Hα. Our survey combines the $z = 2.23$ Hα emitters from HiZELS (Sobral et al. 2013) with Lyα measurements using a custom-made NB filter (see Fig. 1). Here, we describe the first CALYMHA observations from our pilot survey. Section 2 describes the observations, data reduction and photometry. In Section 3, we select emission line candidates, explore their nature and diversity and select our sample of Lyα emitters at $z = 2.23$. Section 4 presents the methods and corrections used in this paper. Section 5 presents the Lyα luminosity function, its evolution and the Lyα EW distribution. In Section 6, we present the results on the Lyα escape fraction and discuss them. Finally, Section 7 presents the conclusions. We use a ΛCDM

Table 1. Observation log of all NB392 observations for our CALYMHA survey, including observations undertaken under bad seeing conditions which were not used. t_{exp} is the total exposure time, while the value between brackets is the exposure time effectively used after rejecting all bad frames. We also show the full range of FWHM in all images for each pointing, while in brackets we show the FWHM within the frames that were effectively used (corresponding to the total exposure times also presented in brackets).

Field	RA (J2000)	Dec. (J2000)	t_{exp} (used) (ks)	FWHM (used) (arcsec)	Dates of observations (All conditions)
COSMOS 1	10 01 59.4	+02 27 06.5	28.4 (8.9)	2.1 ± 0.4 (1.8 ± 0.2)	2014 Feb 28, Mar 1–4
COSMOS 2	10 01 59.4	+01 53 48.5	41.1 (12.9)	3.4 ± 1.2 (1.7 ± 0.1)	2014 Mar 6, 8; 2015 Jan 19–21, 24
COSMOS 3	10 01 15.0	+02 49 18.5	40.0 (21.5)	3.4 ± 1.3 (1.7 ± 0.1)	2014 Mar 5, 7; 2015 Jan 21–24
COSMOS 4	10 00 30.6	+02 16 00.5	105.6 (55)	1.9 ± 0.5 (1.6 ± 0.1)	2014 Mar 1, 7–9, 26, Dec 23–26; 2015 Jan 20–22, 28
COSMOS 5	09 59 46.3	+01 53 48.5	68.7 (11.9)	3.3 ± 1.3 (1.8 ± 0.2)	2014 Mar 4–7, 24–28; 2015 Jan 20, 24, 25
COSMOS 6	09 58 55.7	+02 38 12.5	104.3 (12.2)	2.7 ± 0.9 (1.8 ± 0.1)	2014 Dec 21, 23–25; 2015 Jan 19, 23–28
COSMOS 7	09 58 17.5	+02 04 54.5	49.8 (12.1)	2.2 ± 1.4 (1.9 ± 0.1)	2014 Feb 26–28; Mar 1; 2015 Jan 27–28
UDS 1	02 16 43.0	−04 51 48.0	81.0 (36.0)	2.0 ± 0.9 (1.5 ± 0.2)	2014 Feb 28, Mar 1, 3, Dec 20, 22–25; 2015 Jan 20–27

cosmology with $H_0 = 70\,\mathrm{km\,s^{-1}\,Mpc^{-1}}$, $\Omega_M = 0.3$ and $\Omega_\Lambda = 0.7$. Magnitudes are measured in 3 arcsec diameter apertures in the AB system, unless noted otherwise.

2 OBSERVATIONS AND DATA REDUCTION

2.1 Observations with INT/WFC

Observations were obtained with a custom-built narrow-band filter (NB392) for the Isaac Newton Telescope's Wide Field Camera (INT/WFC). The NB392 filter ($\lambda_c = 3918$ Å, $\Delta\lambda = 52$ Å) was designed by us such that the transmission of the redshifted Lyα line matches that of the redshifted Hα line in the NB$_K$ filter (see Fig. 1). The filter was designed to have an Hα-selected sample as the primary science driver, and thus one requirement was that the filter profile was slightly wider in redshift, so that Hα emitters would have close to 100 per cent transmission in the Lyα filter and also to allow for velocity offsets between Lyα and Hα (see Fig. 1 and Matthee et al. 2016b). First light was obtained on 2013 May 6, and the last observations presented in this paper were taken on 2015 January 27. In total, we have observed for roughly 50 nights (programmes: 2013AN002, 2013BN008, 2014AC88, 2014AN002, 2014BN006, 2014BC118) over a wide range of observing conditions. A significant amount of time was lost due to clouds, high humidity, rain, snow, ice, Sahara dust ('calima') and technical failures. With a typical seeing at La Palma/INT of about 1.3–1.5 arcsec over our observing runs, and with the filter being at short wavelengths (u band), the median seeing is 1.8 arcsec overall in our NB392 filter. Table 1 presents the observations.

Observations were conducted following a cross-dither-pattern, each consisting of five exposures with typical offsets of 30 arcsec to fill in the chip gaps (see Fig. 2) and sample the location of bad/hot pixels in an optimal way. The exposure times for individual frames were either 0.2 or 1.0 ks, depending on whether there was a suitable guide-star available. Autoguiding was relatively challenging because the guide window also goes through our particularly narrow filter, such that a star needs to be about 5–6 mag brighter than usual to provide high enough signal to noise.

2.2 Data reduction: NB392

We reduced our NB392 data with a dedicated pipeline based on PYTHON, presented in Stroe et al. (2014) and Stroe & Sobral (2015). Briefly, the data for each CCD were processed independently. The flats for each night were median combined, after masking sources, to obtain a 'master-flat'. A 'master-bias' for each night of observing was obtained by median-combining biases. The individual exposures were bias-subtracted and sky-flattened to remove electronic camera noise, shadowing effect and normalized for the pixel quantum efficiency. Science exposure pixels that deviated by more than 3σ from the local median were masked. These are either bad pixels (non-responsive) or hot pixels (typically stable over time) or cosmic rays (varying from frame to frame).

We have removed all frames with insufficient quality for our analysis. This included automatic removal of images which had failed astrometry due to the low number of sources in the image, mostly due to high extinction by clouds. We also rejected images for which any problems may have happened, including focusing and read-out issues. We visually checked all frames and removed a total of 20 frames due to read-out errors, guiding losses and satellite trails. These account for the removal of 2 per cent of data.

Our observations were conducted in a wide variety of observing conditions. Before combining the data, we study the effect of different rejection criteria in terms of seeing, such that the depth is maximized. We use SEXTRACTOR (Bertin & Arnouts 1996) to measure the median seeing and then stack frames in ranked sub-sets up to a certain full width at half-maximum (FWHM) seeing. We find that the depth (measured in apertures of 3 arcsec) improves rapidly up to seeing 1.8 arcsec for our deepest pointing, COSMOS P4 (see Matthee et al. 2016b). Other fields reach a greater depth by including frames up to a maximum seeing of 2 arcsec. We therefore use these and reject individual frames with seeing greater than 2 arcsec (see Table 1).

Before stacking, we normalize images to the same zero-point (using SDSS u photometry) and match them to the same point spread function (PSF), see Matthee et al. (2016b). We then mask regions in the final stacks which are too noisy, are contaminated by bright stars or where the S/N is significantly below the average (e.g. gaps between detectors). Fig. 2 presents all the NB392 sources detected after masking, with the density of sources scaling with depth achieved in each sub-region. The total area after masking is 1.43 deg^2.

2.3 Photometric calibration and survey depth

The central wavelength of the NB392 filter lies between the u and B bands in the bluest part of the optical (see Fig. 3), and thus we use both bands to estimate the continuum. We start by PSF matching u and B to NB392 (data from CFHT and Subaru; for full details see Matthee et al. 2016b). We use bright unsaturated stars convolved with a Gaussian kernel to the same FWHM (for full details, see Matthee et al. 2016b).

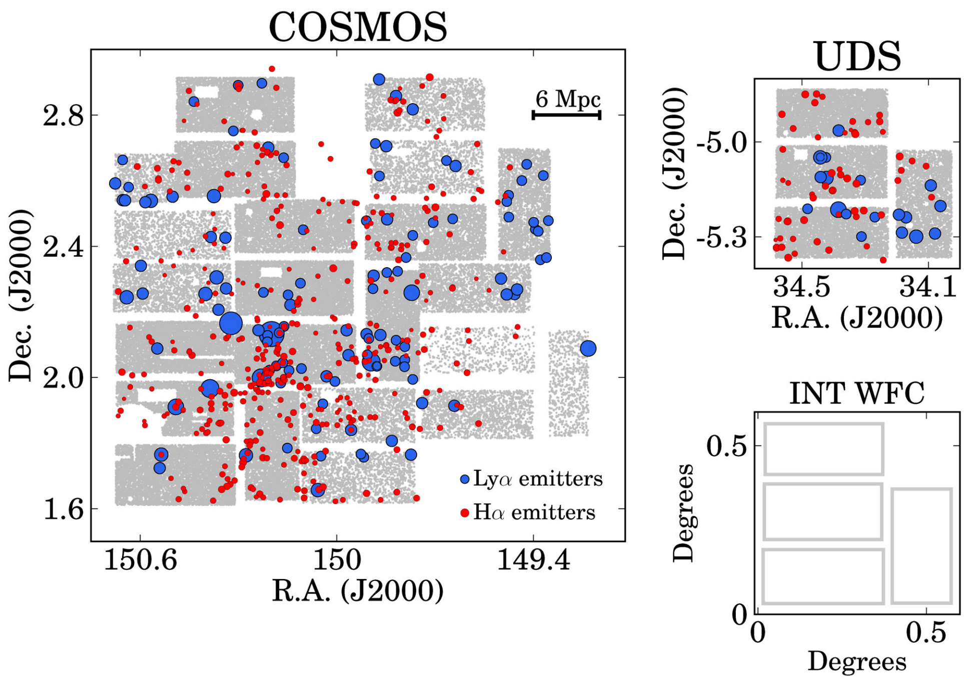

Figure 2. On-sky distribution of all NB392 detections in COSMOS and UDS, showing the masked regions and highlighting the differences in depth of some of the pointings. Grey points show NB392 sources. On top, we show the Hα emitters from Sobral et al. (2013) and our Lyα emitters at $z = 2.23$, after selecting them out of all NB392 emitters (see Section 3.3). Symbol sizes are scaled with luminosity for Lyα emitters. We also show the field of view of WFC/INT. Note that we only cover a fraction of the full UDS field.

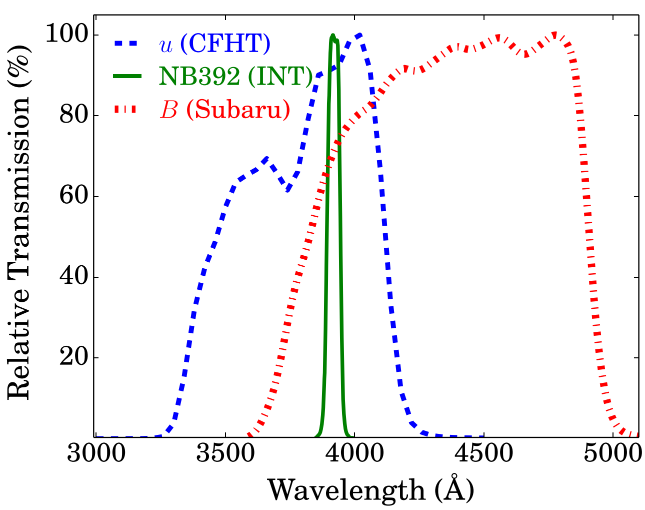

Figure 3. The transmission curves of the u (CFHT), NB392 filter (INT) and B (Subaru) filters used to identify NB392 emitters. We use these three filters for the selection of emitters and to measure emission line fluxes and EWs.

In principle, one could simply use a combination of u and B photometry of several stars in order to calibrate the NB392 data. However, the wavelength range covered by our filter probes the strong stellar CaHK absorption feature, which can vary significantly depending on stellar type and metallicity. Thus, the blind use of stars would introduce significant problems and scatter. In order to solve this potential problem, we use galaxies with photometric redshifts between z = 0.01 and 1.5 without any features in our region of interest, which provide flat, robust calibrators (see Matthee et al. 2016b). We assure this is the case by selecting only galaxies with a flat continuum, i.e. $u - B \approx 0$ colour. We then calibrate the zero-point magnitude for the NB392 data using u with those flat sources in the blue as a first-order calibration.

After calibration, we investigate the final stacked images to study their depths. We do this by placing 100 000 random 3 arcsec apertures in each of the frames (resulting from combining different independent cameras per pointing). We check that the distribution peaks at 0, consistent with a very good sky subtraction. We then measure the standard deviation which we transform into a magnitude limit (1σ). We find that the deepest images are found in COSMOS P4, reaching $M_{392} = 25.0$ (3σ). The average depth over our entire COSMOS coverage is $M_{392} = 24.2 \pm 0.4$ (3σ). In UDS, the average depth is similar to COSMOS, but with a lower dispersion as only one WFC pointing was obtained: $M_{392} = 24.4 \pm 0.2$ (3σ). The depth of u and B data (PSF matched to our NB data) are 26.6 and 26.8 in COSMOS (27.2 and 27.4 in their original PSF; e.g. Capak et al. 2007; Muzzin et al. 2013; Santos et al. 2016) and 26.4 and 26.7 in UDS (Lawrence et al. 2007; Santos et al. 2016).

By using our masks, which avoid noisy regions and pixels which are significantly contaminated by bright stars/haloes, we produce an NB392-selected catalogue. We use SExtractor in dual mode to produce our catalogues, and thus obtain PSF-matched photometry in all other bands, including u and B, which we will use to estimate and remove the continuum and find candidate line emitters. In total, we detect 55 112 sources in COSMOS and 16 242 in UDS in our narrow-band images. All NB392-detected sources are shown in Fig. 2.

2.4 Multiwavelength catalogues and photometry

By using the NB392 image as a detection image, we obtain *uBVgrizJHK* photometry in COSMOS (Capak et al. 2007; McCracken et al. 2012) and UDS (Lawrence et al. 2007). We use these excellent

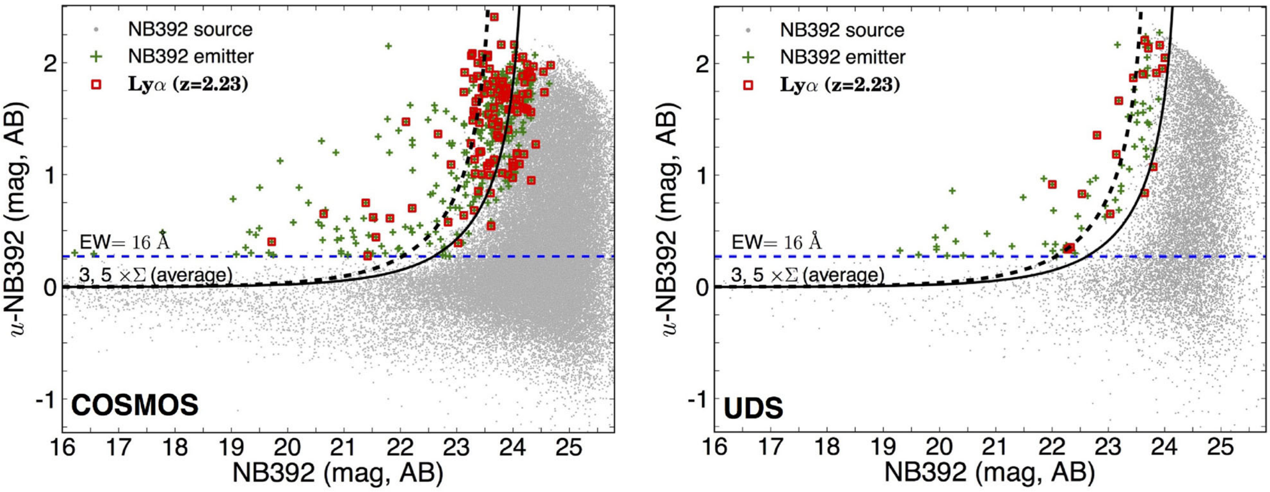

Figure 4. Left: selection of potential line emitters in the full COSMOS field (corresponding to about six INT/WFC pointings; see Fig. 2). We select these as sources with a significant colour excess ($\Sigma > 3$) and with an observed EW > 16 Å. After excluding spurious sources, we find 360 potential line emitters. Note that the COSMOS field coverage contains sub-fields which are significantly deeper than others, and thus our Σ cut in the figure is indicative only of the average depth: some regions will be deeper, while others are shallower. Our actual selection is done on a chip by chip basis. Also, note that at bright magnitudes, the prevalence of stars, with CaHK absorption features, makes many bright sources have a negative u − NB392 colour, as a result of this absorption. Right: the similar selection diagram for the UDS field, targeted with a single WFC/INT pointing (see Fig. 2). We apply the same selection criteria to COSMOS ($\Sigma > 3$ and EW > 16 Å). We find 80 candidate line emitters.

data for colour–colour selection in this paper, assuring we measure the photometry from all NB392 sources, even if they result in non-detections/upper limits. Furthermore, we also use publicly available catalogues of the COSMOS field (Ilbert et al. 2009) and the UDS field (Cirasuolo et al. 2010), including a large amount of spectroscopic and photometric redshifts (see also Sobral et al. 2013).

3 NB392 AND LYα EMITTERS SELECTION

3.1 Excess selection: Σ and EW cuts

We correct for any potential dependence of excess on $u - B$ colours (see Fig. 3) by selecting spectroscopically confirmed galaxies which have no features at the observed 3920 Å. In practice, we empirically correct the NB magnitude using:

$$\mathrm{NB392} = \mathrm{NB392}_{\mathrm{uncorrected}} + 0.19 \times (u - B) - 0.09. \tag{1}$$

This correction ensures that a zero NB excess translates into a zero line flux in NB392. For sources which are undetected in u or B, we assign the median correction of the sources that are detected in u and B: +0.02. We note that our corrections empirically tackle potential effects from IGM absorption without any uncertain model assumptions (see e.g. Vasei et al. 2016); but see other studies that correct for IGM effects differently (e.g. Ouchi et al. 2008; Konno et al. 2016). This is because, in general, a source with significant IGM absorption (blueward of Lyα) will end up with a redder $u - B$ colour than a source with e.g. little to no IGM absorption at all. If only the u band was used, and significant IGM absorption happens, the total continuum flux we would measure (spread over the full u filter) would be an average over the filter, and thus would be an underestimate of the real continuum flux at Lyα. Our correction is able to correct for that.

In order to robustly select sources that have a likely emission line in the NB392 filter, including Lyα emitters at $z = 2.23$, we need to find sources which show a real colour excess of the narrow-band (NB392) over the broad-band (in the following, we refer to the broad-band u as BB). This is to avoid selecting sources that may mimic such excess due to random scatter or uncertainty in the measurements. In practice, this is assured by using two different selection criteria:

(i) a significance cut ($\Sigma > 3$);
(ii) an equivalent width cut (EW > 16 Å; u-NB392 > 0.3).

The parameter Σ (e.g. Bunker et al. 1995) is used to quantify the real excess compared to an excess due to random scatter. This means that the difference between counts in the narrow-band and the broad-band must be higher than the total error times Σ. It can be computed using (Sobral et al. 2013)

$$\Sigma = \frac{1 - 10^{-0.4(\mathrm{BB-NB})}}{10^{-0.4(\mathrm{ZP-NB})}\sqrt{(\sigma_{\mathrm{NB}}^2 + \sigma_{\mathrm{BB}}^2)}}. \tag{2}$$

Here, ZP is the zero-point of the narrow-band (NB), NB392, which is the same as the PSF-matched u-band data (BB); both are scaled to ZP = 30 in our analysis. We classify as potential emitters the sources that have $\Sigma > 3$ (see Fig. 4), following Sobral et al. (2013).

The second criterion for an excess source to be an emitter is that the emission line must have an observed-frame EW (the ratio of the line flux and the continuum flux densities) higher than the scatter at bright magnitudes. This step avoids selecting sources with highly non-uniform continua (with e.g. strong continuum features). We compute EWs by using

$$\mathrm{EW} = \Delta\lambda_{\mathrm{NB}} \frac{f_{\mathrm{NB}} - f_{\mathrm{BB}}}{f_{\mathrm{BB}} - f_{\mathrm{NB}}(\Delta\lambda_{\mathrm{NB}}/\Delta\lambda_{\mathrm{BB}})}, \tag{3}$$

where $\Delta\lambda_{\mathrm{NB}} = 52$ Å and $\Delta\lambda_{\mathrm{BB}} = 720$ Å are the widths of the filters and f_{NB} and f_{BB} are the flux densities for the narrow-band (NB392) and broad-band (u), respectively. In order to identify a source as a potential line emitter, we require it to have EW (observed) higher than 16 Å, corresponding to an excess of u − NB392 > 0.3 (>3 times the scatter at bright magnitudes). Note that this will correspond to different rest-frame EWs depending on the line/redshift being

Table 2. Our NB392 filter ($\lambda_c = 3918$ Å, $\Delta\lambda = 52$ Å) is sensitive to a range of emission lines. Here, we list the most prominent (see Fig. 5, which shows these lines in comparison with photometric and spectroscopic redshifts). The redshift (z) range shown corresponds to the FWHM of the filter profile. We note that broad emission lines will be picked up over a larger redshift range, and that there may be other, rarer, emission lines, which may also be picked up by our survey. Also, we note that the current spectroscopy is particularly biased towards the UV bright and AGN sources. Fractions given are out of the total number of sources with a robust spectroscopic redshift.

Feature/line (rest-frame, Å)	Redshift (z)	# (%) in sample (from $z_{\rm spec}$)
[O II]$_{3727}$	0.044–0.058	8 (14)
[Ne V] $_{3426,\,3346}$	0.136–0.179	2 (4)
Mg I $_{2853}$	0.364–0.382	3 (6)
Mg II $_{2799}$	0.390–0.409	0 (0)
[Ne IV] $_{2425}$	0.605–0.626	2 (4)
C III] $_{2326}$	0.673–0.696	3 (6)
C III] $_{1909}$	1.039–1.066	6 (11)
He II $_{1640}$	1.373–1.405	4 (7)
C IV $_{1549}$	1.513–1.546	14 (25)
N V $_{1239}$	2.141–2.183	2 (4)
Lyα $_{1216}$	**2.201–2.243**	10 (19), 17 (NB)

Table 3. Summary of the information in our CALYMHA catalogue. When available, the number of spectroscopic redshifts are shown as well. The number of Lyα emitters within brackets are those with high S/N continuum detections, allowing to be robustly selected using either photometric redshifts or colour–colour selections. We provide the catalogue of all 440 line emitters in Appendix A. Out of our 188 Lyα emitters, 13 have a robust detection of either [O II], [O III] or Hα. See also Matthee et al. (2016b) for discussion of Lyα properties of 17 Hα emitters recovered down to lower Σ in our NB392 data.

Sample	No. of sources	z-spec.
NB392 detections: COSMOS	55 112	5683
NB392 detections: UDS	16 242	801
Emitters (before visual check)	477	70
Emitters (after visual check)	440	70
Lyα emitters $z = 2.23$	188 (142)	17

looked at. We note that specifically to select Lyα emitters at $z = 2.23$, our EW cut corresponds to $\rm EW_0 > 5$ Å, which is well below the traditional cut of $\rm EW_0 > 25$ Å (e.g. Ouchi et al. 2008) for 'Lyα emitters'. This is usually enforced by the typical narrow-band filter widths that do not allow studies to go down to lower EWs. However, this is not the case for our study as we use a narrower filter, and we thus take advantage of that to explore lower EWs.

Fluxes of all emission lines are calculated as follows:

$$F_{\rm line} = \Delta\lambda_{\rm NB}\frac{f_{\rm NB} - f_{\rm BB}}{1 - (\Delta\lambda_{\rm NB}/\Delta\lambda_{\rm BB})}, \tag{4}$$

with each parameter having been previously defined.

Using our selection criteria, out of the 55 112 NB392 sources individually detected in COSMOS, 394 emitters were selected as potential line emitters (0.7 per cent). For UDS, out of the 16 242 NB392 detections, we identify 83 candidate line emitters (0.5 per cent). However, some of these may still be artefacts and/or sources in very noisy regions. We therefore clean our list of potential emitters by visually inspecting all candidates before flagging them as final emitters and produce a final mask. This leads to a sample of 360 and 80 potential emitters in COSMOS and UDS, respectively, yielding a total of 440 candidate line emitters (see Fig. 4, Tables 3 and A2), covering an effective area of 1.43 deg^2 after our conservative masking (see Fig. 2).

Table 2 indicates the major emission lines expected to be found with our narrow-band filter. In the following sections, we explore the wealth of multiwavelength data, photometric and spectroscopic redshifts and colour–colour selections, in order to select Lyα emitters at $z = 2.23$ (see Fig. 2 and Table 3), but also to identify other emission lines. We present a catalogue with all line emitters, and those which we class as likely Lyα emitters in Appendix A.

3.2 Photometric and spectroscopic redshifts of candidate NB392 line emitters

We show the photometric redshift (Ilbert et al. 2009; Cirasuolo et al. 2010) distributions of the candidate NB392 line emitters in Fig. 5. We have photometric redshifts for 287 out of our 440 NB392 candidate line emitters (65 per cent). The remaining are typically very faint in the continuum ($i > 26$). We note that the photometric redshifts have been derived with a large range of models, including emission lines, AGN and also stars.

The photometric redshift distribution for the sources for which we have a reliable photometric redshifts, shows tentative peaks associated with strong lines expected to be detected, as detailed in Table 2, including Lyα at $z = 2.23$, but also [O II]$_{3727}$, Mg I$_{2853}$, C III]$_{1909}$, He II$_{1640}$ and C IV$_{1549}$ (see Fig. 5). The photometric redshifts hint that while the sample of emitters is dominated by Lyα emitters, high excitation Carbon line emitters seem to be an important population.

Spectroscopic redshifts are also available for ∼16 per cent of the selected line emitters (e.g. Yamada et al. 2005; Simpson et al. 2006; van Breukelen et al. 2007; Geach et al. 2007; Ouchi et al. 2008; Smail et al. 2008; Lilly et al. 2009; Ono et al. 2010a; Civano et al. 2012, 2016; Khostovan et al. 2016; Sobral et al. 2016), and we show the distribution of those redshifts, for our sample of NB392 line emitters, in Fig. 5. We note that these heterogeneous compilations of redshifts do not allow us to derive robust quantitative conclusions. This is because different spectroscopic surveys have very different selections, and in general they are biased towards the optically brighter sources and/or they result from the follow-up of AGN sources. Also, most surveys do not have the blue sensitivity to detect Lyα at $z \sim 2$, and thus the spectroscopically confirmed Lyα emitters are mostly obtained through other AGN lines. Regardless, one can clearly identify the major emission lines one would expect. We find results that are consistent with the distribution of photometric redshifts.

3.3 Selecting Lyα emitters at $z = 2.23$

The selection of Lyα emitters at $z = 2.23$ follows Sobral et al. (2013), using a combination of photometric redshifts (and spectroscopic redshifts, when available) and colour–colour selections optimized for star-forming galaxies at the redshift of interest ($z \sim 2.2$). We note that such selection criteria are optimized for $z \sim 2.2$ independently of galaxy colour. In fact, as shown in Oteo et al. (2015), Hα emitters as selected in Sobral et al. (2013) span the full range of galaxy colours expected at $z = 2.23$, from the bluest to the reddest galaxies.

As can be seen in Fig. 5, the photometric redshift distribution can provide a very useful tool to select $z = 2.23$ Lyα emitters, for relatively bright optical sources. However, photometric redshifts can be highly uncertain, and have significant systematics, particularly at $z \sim 2$ and for blue sources. This is important as many Lyα

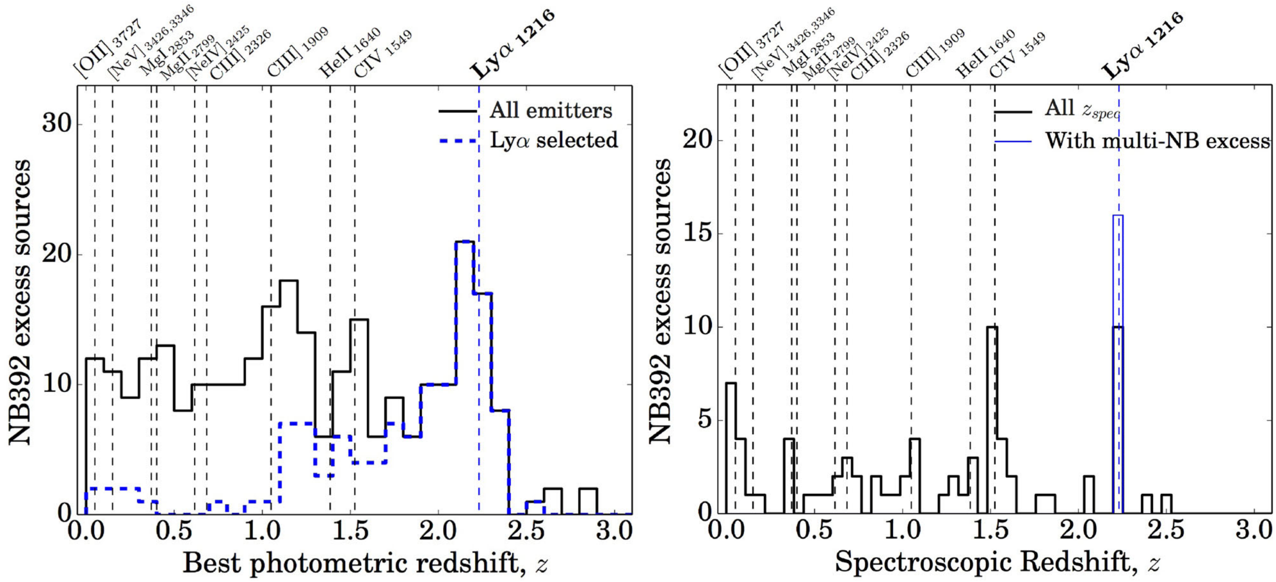

Figure 5. Left: the distribution of photometric redshifts for our candidate NB392 line emitters, indicating the redshift of major emission lines – see Table 2. We find that tentative photometric redshift peaks at the redshifts expected from major emission lines. Note that a fraction of the sources (∼30 per cent) is too faint in the continuum to derive a photometric redshift, and thus is not shown here. For those with a photometric redshift, there is evidence that while Lyα emitters dominate, there is a significant population of C IV and C III] emitters, followed by Mg emitters, and Ne V + [O II] emitters. Right: the distribution of spectroscopic redshifts for our sample, from heterogeneous compilations and mostly i-band-selected spectroscopic surveys. Even though the spectroscopic redshifts available from the literature are not representative of the full sample, and are highly biased towards AGN, the results agree fairly well with the photometric redshift distribution, revealing 5–10 spectroscopic confirmations of all major lines. We also show the NB392 emitters which are emitters in either NB$_J$, NB$_H$ and/or NB$_K$ (from Sobral et al. 2013, see Section 3.3), which can be considered as spectroscopically confirmed.

emitters are expected to be very blue. Furthermore, photometric redshifts are not available for a significant fraction (∼30 per cent) of the typically fainter NB392 emitters. Thus, relying solely on photometric redshifts would not result in a clean, high completeness sample of z = 2.23 Lyα emitters. We mitigate this by following Sobral et al. (2013), i.e. by applying colour–colour selections for the fainter NB392 emitters (see Section 3.3.2). We also discuss the selection of the faintest sources, which are undetected in the continuum in Section 3.3.2.

While spectroscopy is extremely limited for z = 2.23 sources, double, triple and quadruple narrow-band line detections between NB392 and NB$_K$ (Hα), NB$_H$ ([O III]) and/or NB$_J$ ([O II]) can be very useful if these lines are bright enough in the observed NIR (Sobral et al. 2013). Those allow the identification of further seven secure Lyα emitters, while they also recover six out of the 11 spectroscopically confirmed ones, including one source that is an emitter in all narrow-bands (see Matthee et al. 2016b). Overall, 13 Lyα emitters have information for at least another line from multi-narrow-band imaging (see Fig. 5). Note that Matthee et al. (2016b) present a larger number of Lyα+Hα emitters, as the study goes down to lower significance in the NB392 filter, by focusing on the Hα emitters from Sobral et al. (2013).

3.3.1 Selecting continuum-undetected Lyα emitters

We note that out of all 440 line emitters, 387 are ‘selectable’ (≈88 per cent), i.e. we either have a photometric redshift (65 per cent) or $B-z$ and $z-K$ colours (88 per cent) that will allow us to test whether they are Lyα emitters in Section 3.3.2. For the remaining 53 sources (12 per cent) this is not possible. We investigate these 53 sources, finding that they present the lowest emission line fluxes in the sample, but, having faint or non-detectable continuum in redder bands than u, they have typically very high EWs (median observed EWs ≈300 Å), consistent with the majority being Lyα emitters at z = 2.23 (simultaneously the only line able to produce such high EWs and the higher redshift line). For these sources, we apply the canonical EW$_0$ > 25 Å (z = 2.23), which selects 46 out of the 53 sources, and flag these as candidate Lyα emitters, including them in our sample (see also Rauch et al. 2008). We note that they all have Lyα luminosities in the range $10^{42.5\pm0.2}$ erg s^{-1}, and contribute to the very faintest bin in the Lyα luminosity function. The remaining/excluded seven sources have lower EWs, likely explained by very low mass lower redshift emitters, such as C III] emitters, although we note that they can still be Lyα emitters (adding these seven sources does not change any of our results).

In summary, we identify 46 sources as Lyα emitters out of the 53 which are not detected in broad-bands.

3.3.2 Selecting continuum-detected Lyα emitters

The selection of Lyα emitters is identical for our COSMOS and UDS fields, and we follow the selection criteria of Sobral et al. (2013). An initial sample of z = 2.23 Lyα emitters is obtained by selecting sources for which 1.7 < $z_{\rm phot}$ < 2.8. This selects 77 sources, of which three are spectroscopically confirmed to be contaminants, four are spectroscopically confirmed z = 2.23 and 11 are double/triple narrow-band excess sources and thus robust z = 2.23 Lyα emitters. Because some sources lack reliable photometric redshifts, the colour selection ($z-K$) > ($B-z$) is used to recover additional $z\sim2$ continuum-faint emitters. This colour–colour selection is a slightly modified version of the standard BzK (Daddi et al. 2004) colour–colour separation (see Sobral et al. 2013). It selects 70 additional Lyα candidates (and re-selects 73 per cent of those selected through photometric redshifts; four sources are

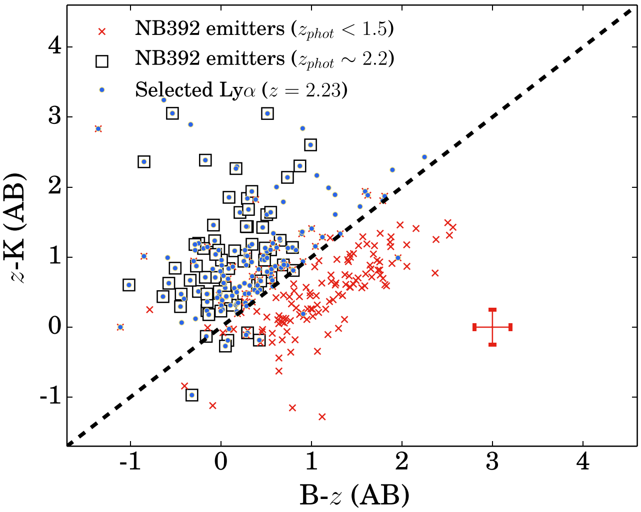

Figure 6. In addition to using photometric and spectroscopic redshifts, and in order to increase our completeness, we also use the *BzK* colour–colour selection to select Lyα emitters, following Sobral et al. (2013). This allows us to select fainter line emitters for which photometric and spectroscopic redshifts are not available. Note that some real Lyα emitters are slightly outside the selection region, but are recovered by either spectroscopic redshifts or by dual/triple line detections; these are typically AGNs.

contaminants, two are $z = 2.23$ Lyα emitters), and guarantees a high completeness of the Lyα sample (see Fig. 6). Finally, two spectroscopically confirmed Lyα sources (AGN, from C-COSMOS) are also selected, which are missed by the photometric redshift and colour–colour selection due to the unusual colours (these are also double/triple narrow-band excess sources). *BzK* also selects much higher redshift sources, which can be a source of contamination for the Hα selection at $z = 2.23$ with the NB$_K$ filter (e.g. oxygen lines, see Sobral et al. 2013). This is not a problem for NB392, as no strong emission lines make it into the filter at wavelengths bluewards of Lyα.

Overall, we identify 142 Lyα emitters (see Table 3) which are directly selected, along with the other 46 candidate Lyα emitters that are very faint and/or undetected in the continuum. Our final sample is thus made of 188 Lyα emitters.

With the limited spectroscopy available, it is difficult to accurately determine the completeness and contamination of the sample. However, based on the double/triple narrow-band excess detections and spectroscopically confirmed Lyα emitters (15 are selected out of a total of 17), we infer a likely completeness of $\approx$90 per cent. Of all of the sources initially selected as Lyα emitters ($\sim$60 per cent of NB392 excess sources are not selected as Lyα emitters). Amongst these, seven were contaminants (now removed), dominated by C IV and C III] emitters. As discussed above, there are reasons to suspect that a larger fraction of the contaminants will have available redshifts (e.g. AGN), and thus we estimate a contamination of between about 5 and 10 per cent.

4 METHODS AND CORRECTIONS

4.1 Lyα luminosity function calculation

4.1.1 Completeness corrections

Faint sources and those with weak emission lines and/or low EW might be missed in our selection and thus not included in the sample and/or in a particular sub-volume within our survey. The combination of such effects will result in the underestimation of the number of Lyα emitters, especially at lower luminosities. In order to account for that, we follow the method described in Sobral et al. (2013) to estimate completeness corrections per sub-field per emission line.

Very briefly, we use sources which have not been selected as line emitters ($\Sigma < 3$ or EW < 16 Å), but that satisfy the selection criteria used to select Lyα (photometric and colour–colour selection). We then add emission line flux to all those sources, and study the recovery fraction as a function of input flux. We do these simulations in a sub-field by sub-field basis. We then apply those corrections in order to obtain our completeness-corrected luminosity functions. We note that in order to deal with the significant differences in depth across our survey areas, and in order to produce robust results, when evaluating the Lyα luminosity function, we only take into account sub-volumes (per chip) if, for that bin, they are complete at a >50 per cent level.

4.1.2 NB392 filter profile corrections

The NB392 filter transmission function is not a perfect top-hat (see Fig. 1). Therefore, the real volume surveyed is a weak function of intrinsic luminosity. This is a much stronger effect for filters, which are much more Gaussian, such as the NB$_K$ filter (see Fig. 1). For example, luminous line emitters will be detectable over a larger volume (even though they will seem fainter) than the fainter ones, as they can be detected in the wings of the filter. Conversely, genuine low-luminosity sources will only be detectable in the central regions of the filter, leading to a smaller effective volume. In order to correct for this when deriving luminosity functions, we follow the method described in Sobral et al. (2012). Briefly, we compute the luminosity function assuming a top-hat narrow-band filter. We then generate a set of 10^6 line emitters with a flux distribution given by the measured luminosity function, but spread evenly over the redshift range being studied (assuming no cosmic structure variation or evolution of the luminosity function over this narrow redshift range). We fold the fake line emitters through the top-hat filter model to confirm that we recover the input luminosity function perfectly. Next, we fold the fake line emitters through the real narrow-band profiles – their measured flux is not only a function of their real flux, but also of the transmission of the narrow-band filter for their redshift. The simulations show that the number of brighter sources is underestimated relative to the fainter sources. A mean correction factor between the input luminosity function and the one recovered (as a function of luminosity) was then used to correct each bin. In practice, the corrections range from a factor of 0.97 in the faintest bin to 1.3 in the brightest bin.

4.2 NB392/NB$_K$ filter profile ratios: corrections in measuring Lyα/Hα ratios

As we will compare Lyα and Hα directly to obtain line ratios, we derive corrections due to the use of the specific filter profiles. By design, our sample of Lyα emitters have their Hα emission in the HiZELS NB$_K$ filter (see Fig. 1). Therefore, it is possible to measure Lyα/Hα ratios directly. However, the slightly different filter transmission and velocity offsets between Hα and Lyα can introduce biases (see Fig. 1 and discussion in Matthee et al. 2016b).

We obtain the average relative transmission between Lyα and Hα for Lyα-selected sources similarly as described in (Matthee et al. 2016b, see also e.g. Nakajima et al. 2012). We simulate

100 000 Lyα emitters with a redshift probability distribution given by the NB392 filter transmission, as our sample is NB392 (Lyα) selected. Note that in Matthee et al. (2016b), the sample is NB$_K$ (Hα) selected, and thus the redshift probability distribution is given by the NB$_K$ filter, leading to different filter corrections. Assuming a dispersion of velocity offsets with a median of 200 km s^{-1} (e.g. Steidel et al. 2010; Hashimoto et al. 2013; Stark et al. 2013; Erb et al. 2014; Song et al. 2014; Sobral et al. 2015b), we measure the transmission for the redshifted Hα line in the NB$_K$ filter and thus obtain the relative transmission between Lyα and Hα. We find that the Lyα transmission is on average ≈1.7 times higher than Hα (see Fig. 1), due to the more top-hat-like shape of the NB392 filter as compared to the NB$_K$ filter; i.e. many Lyα emitters (Lyα selected) are observed in the wings of the NB$_K$ filter. We correct for this relative transmission in all our measurements of the Lyα escape fraction, $f_{\rm esc}$. This is a robust correction as long as our Lyα sample has a redshift distribution given by the NB392 filter profile.

We show how the measured line ratio changes as a function of redshift in Fig. 1. We note that the overestimation of the Lyα/Hα ratio, for a Lyα-selected sample, is particularly high towards the wings of the filter and is very uncertain on a source by source basis. Therefore, for the remainder of this paper, we only use Lyα/Hα ratios obtained by stacking either the full sample of Lyα emitters, or sub-samples, and apply the statistical correction we derive, by dividing observed Lyα/Hα ratios by 1.7.

4.3 Stacking and Lyα escape fraction from Lyα/Hα

The observed fraction of Lyα to Hα flux encodes information on the fraction of Lyα photons that escape a galaxy, $f_{\rm esc}$. Under the assumption of case B recombination, a temperature of $T \approx 10^4$ K and electron density of $n_{\rm e} \approx 350$ cm^{-3}, the intrinsic ratio of Lyα to Hα photons is expected to be 8.7 (see e.g. Hayes 2015 for a recent review and for a discussion on how sensitive this number is to a range of physical conditions). The departure of this ratio is defined as the Lyα escape fraction, $f_{\rm esc} = L_{{\rm Ly}\alpha}/(8.7\,L_{{\rm H}\alpha})$, where $L_{{\rm H}\alpha}$ is corrected for dust attenuation.

We measure the median $f_{\rm esc}$ of our sample of Lyα emitters by stacking the PSF-matched U, B, NB392, NB$_K$ and K images on the positions of Lyα emitters, following the same methodology as in Matthee et al. (2016b). Photometry is measured in 3 arcsec diameter apertures and line fluxes are computed as described in Section 3.1. We correct for dust extinction/dust affecting the Hα line by using the median extinction $A_{{\rm H}\alpha} = 0.9$ (see e.g. Sobral et al. 2012; Ibar et al. 2013; Sobral et al. 2013; Matthee et al. 2016b) and correct the observed Lyα/Hα ratio for the relative filter transmission, as described in Section 4.2.

5 RESULTS

5.1 Lyα luminosity function at $z = 2.23$: comparison to other surveys and evolution

We estimate source densities in a luminosity bin of width $\Delta(\log L)$ centred on $\log L_{\rm c}$ by obtaining the sum of the inverse volumes of all the sources in that bin, after correcting for completeness. The volume probed is calculated taking into account the survey area and the narrow-band filter width, followed by applying the appropriate real filter profile corrections obtained in Section 4.1.2.

The luminosity functions presented here are fitted with Schechter functions defined by three parameters: α (the faint-end slope), L^* (the transition between a power law at lower luminosities and an exponential decline at higher luminosities) and ϕ^* (the number density/normalization at L^*). We can still get a reasonable constraint on α, but we also fit the luminosity function by fixing α to common values found in the literature ($\alpha = -1.5, -1.7$; e.g. Ouchi et al. 2008; Hayes et al. 2010; Konno et al. 2016), particularly so we can make a direct comparison. Finally, we also explore power-law fits with the form: $\log_{10}\phi = A \times \log_{10}(L) + B$.

We present our final $z = 2.23$ Lyα luminosity function in Fig. 7 and in Table A1. We find it to be well fit by a Schechter function up to $10^{43.0}$ erg s^{-1}. Our best-fitting parameters for $L < 10^{43.0}$ erg s^{-1} are

$$\log L^*_{{\rm Ly}\alpha} = 42.59^{+0.16}_{-0.08}\,{\rm erg\,s^{-1}}$$

$$\log \phi^*_{{\rm Ly}\alpha} = -3.09^{+0.14}_{-0.34}\,{\rm Mpc^{-3}}$$

$$\alpha_{{\rm Ly}\alpha} = -1.75 \pm 0.25.$$

Our results favour a steep α for the Lyα luminosity function at $z = 2.23$ ($\alpha \approx -1.8$), in very good agreement with Konno et al. (2016). Beyond $10^{43.0}$ erg s^{-1}, we find evidence of a significant deviation from a Schechter function, similarly to what was found by Ouchi et al. (2008) and Konno et al. (2016). We thus fit a power law ($\log_{10}\phi = A \times \log_{10}(L) + B$), with parameters $A = -1.48$ and $B = 59.4$. We show our results and the best fits in Fig. 7. We also attempt to fit a single power law to our full Lyα luminosity function. The best fit yields a reduced $\chi^2 = 1.4$ with $A = -1.9 \pm 0.2$ and $B = 79 \pm 6$.

We compare our results with other studies at $z = 2.23$ (e.g. Hayes et al. 2010; Konno et al. 2016). We correct the Konno et al. (2016) data points for potential contamination (particularly important at the bright end; see Section 5.2), but we also show the Schechter fit derived without such corrections; see Fig. 7. We find very good agreement with Konno et al. (2016) across most luminosities regardless of the contamination correction (CC), but after such correction our results agree at all luminosities. We find a higher number density of Lyα emitters at comparable luminosities than Hayes et al. (2010), but we note that we probe a significantly larger volume (≈150 times larger), and thus cosmic variance is likely able to explain the apparent discrepancies (ϕ^* expected to vary by more than a factor of 2 for surveys of the size of theirs; see Sobral et al. 2015a).

We also compare our results with other previous determinations presented in the literature at slightly different redshifts (e.g. Blanc et al. 2011; Cassata et al. 2011; Ciardullo et al. 2012, 2014), finding good agreement. Other studies have made contributions towards unveiling the Lyα luminosity function at $z < 2$ (see e.g. Cowie et al. 2010; Barger et al. 2012). Comparing to these, we find a very strong evolution in the Lyα luminosity function from $z = 0.3$ to 2.23. For $\alpha = -1.6$, the characteristic luminosity evolves by almost 1 dex from $z = 0.3$ to 2.23, a very similar behaviour to the evolution of L^* of the Hα luminosity function (Sobral et al. 2013). ϕ^* evolves by about 0.8 dex, thus much more than the mild ∼0.2–0.3 dex evolution seen for the Hα luminosity function (Sobral et al. 2013).

Comparing our results with higher redshift (e.g. Ouchi et al. 2008, 2010; Matthee et al. 2015; Drake et al. 2016; Santos et al. 2016), we find that the Lyα luminosity function continues to evolve at least up to $z = 3.1$. We note that issues with contamination and/or completeness, due to the simple EW cut usually used may play an important role at $z \sim 3$ and at higher redshift, although it is expected to be less important than at $z \sim 2$.

We note that the bright-end power-law component of the Lyα luminosity function is consistent with being dominated by luminous X-ray AGN. We can conclude this because 10 out of the 12

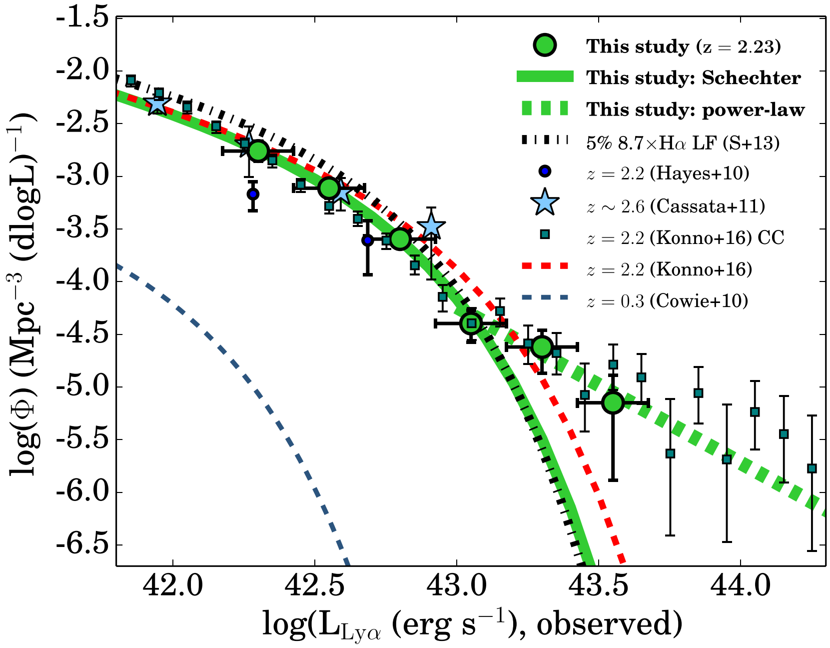

Figure 7. The Lyα luminosity function for our combined COSMOS and UDS coverage and down to a Lyα EW$_0$ > 5 Å. We find that the LF is well fitted by a Schechter function up to $\sim 10^{43}$ erg s^{-1}, but seems to become a power law for higher luminosities. We also show the Lyα luminosity function presented by Hayes et al. (2010) at $z = 2.2$, Cassata et al. (2011) at $z \sim 2.6$ and the recent determination at $z = 2.2$ by Konno et al. (2016) before (dashed red line and Fig. 8) and after our CC (see Section 5.2). We find good agreement with the wide and deep survey of Konno et al. (2016), including the departure from the Schechter function. We are also in very good agreement with Cassata et al. (2011). While it may seem that we are in disagreement with Hayes et al. (2010), we note that their data points, due to probing a very deep, but very small single volume, only overlap with the faintest of our two bins, and there is likely to be strong cosmic variance in their survey. We also show the extinction-corrected Hα luminosity function from Sobral et al. (2013), transformed into Lyα with a 5 per cent escape fraction.

(83 ± 36 per cent) Lyα emitters with $L > 10^{43}$ erg s^{-1} are detected in *Chandra*/X-rays with luminosities in excess of $\approx 10^{43.5}$ erg s^{-1} (Civano et al. 2016). We note that while these sources have significant Lyman-breaks, and all are X-ray sources, two of our Lyα emitters are also candidates for being strong Lyman continuum (LyC) leakers (Matthee et al. 2016a). This is consistent with the potential connection between the escape of Lyα and LyC photons (see e.g. Verhamme et al. 2015, 2016; Dijkstra, Gronke & Venkatesan 2016; Vanzella et al. 2016).

5.2 Lyα luminosity function: how important is it to remove contaminants?

We have presented the Lyα luminosity function at $z = 2.23$ with our robust Lyα-selected sample (see Figs 8 and 7), which goes down to EW$_0$ ≈ 5 Å. We stress that for the highest Lyα luminosities (>10^{43} erg s^{-1}), we have spectroscopic redshifts for 50 per cent of all line emitters. We now investigate the role of selecting Lyα among all narrow-band emitters (see Fig. 8). This is particularly relevant, as most studies until now have made the assumption that contamination from other lines should be negligible. We have already showed how important it actually is in practice when we presented the distribution of photometric and spectroscopic redshifts in Section 3.2, but here we place that into the context of deriving Lyα luminosity functions. This may be particularly relevant to understand and discuss significant differences in results with other studies.

In order to address this issue, we compare our most robust results, after carefully selecting Lyα emitters (and using the wealth of spectroscopic redshifts available), with those we would have derived if we assumed that the sample was dominated by Lyα emitters (as long as we apply a particular EW cut). We show the results in Fig. 8. It is particularly interesting to compare the results from a recent study, which also targeted COSMOS and UDS, with a slightly different filter (Konno et al. 2016). The crucial difference between our study and Konno et al. (2016) is that we use spectroscopic and photometric redshifts, colour–colour selections and take advantage of dual/triple and quadruple narrow-band detections for other emission lines. We thus obtain a very robust sample of Lyα emitters, and exclude confirmed and very likely contaminants. As presented in Section 3.2, down to the flux limit of our study, around ≈50 per cent of the emitters are likely not Lyα, with the bulk of them being C III] and C IV, not [O II]. However, Konno et al. (2016) assume that all narrow-band excess sources above a certain EW correspond to Lyα. While such assumption may work relatively well for very low fluxes, it breaks down at the highest fluxes, as our spectroscopic results show.

In order to compare our results, we apply the EW$_0$ cut (EW$_0$ > 20 Å) of Konno et al. (2016), and no other selection criteria. Based on our spectroscopic redshifts (dominated by sources with fluxes corresponding to $L_{\rm Ly\alpha} > 10^{43}$ erg s^{-1}), this results in a highly contaminated sample at the bright end (16 confirmed contaminants out of 21 sources with spectroscopy; 76 per cent contamination), whilst being relatively incomplete for bright Lyα emitters: only five spectroscopically confirmed Lyα emitters are recovered out of the 11 (completeness ∼45 per cent).

We can now derive a new luminosity function, fully comparable with Konno et al. (2016), which we show in Fig. 8. Our results show a remarkable agreement at all luminosities, and we recover

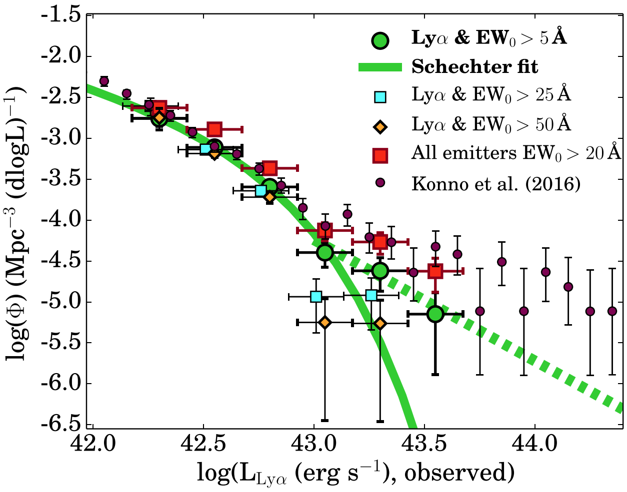

Figure 8. The Lyα luminosity function for our combined COSMOS and UDS coverages down to a Lyα EW$_0 > 5$ Å. We compare with what we would obtain by not removing contaminants, but instead applying only a higher EW cut (EW$_0$ > 20 Å), to directly compare with Konno et al. (2016). We find that we can fully recover the results of Konno et al. 2016, including a much higher number density of very bright sources. However, as our spectroscopic (we have spectroscopic redshifts for 50 per cent of all $>10^{43}$ erg s^{-1} line emitters) and photometric redshift analysis shows, this is driven by the presence of C III] and C IV emitters. We also investigate and show the effect of varying the Lyα EW$_0$ cut in addition to our robust Lyα selection (redshifts and colour–colour selection). For different EW cuts, we re-compute all our completeness corrections per field to take into account that our selection changes (a higher EW cut means a lower completeness, so our completeness corrections increase). We find that completeness corrections can compensate for incompleteness at the faint end, but the bright end becomes significantly incomplete for higher EW cuts.

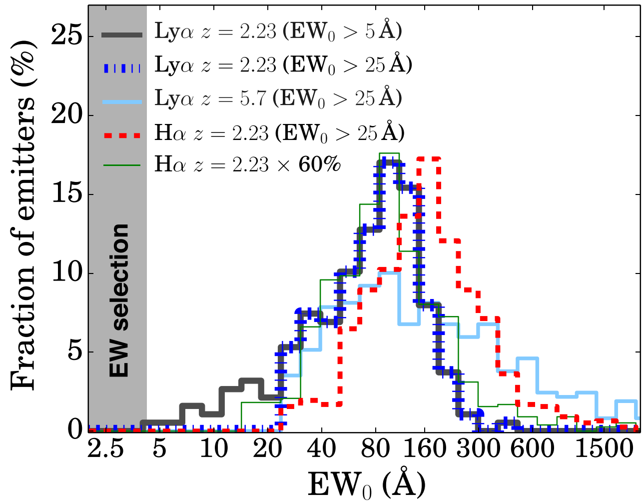

Figure 9. The rest-frame EW distribution of Lyα-selected emitters at $z = 2.23$. We find an average EW$_0 = 85 \pm 57$ Å, with a median of $\approx$100 Å. We find that 11 per cent of all Lyα emitters have $5 <$ EW$_0 < 25$ Å, but that the lower EW$_0$ Lyα emitters are preferentially the brightest in Lyα luminosity, and are particularly important for the bright end of the Lyα luminosity function at $z = 2.23$ (X-ray AGN). We also show the Hα EW$_0$ distribution of Hα emitters from Sobral et al. (2014), from roughly the same volume surveyed with Lyα. This clearly shows that the rest-frame EW distribution of Hα is shifted to higher values, but scaling them by 60 per cent recovers a similar distribution. For comparison at higher redshift, but avoiding potential re-ionization effects, we also show the EW$_0$ of Lyα emitters at $z = 5.7$ from Santos et al. (2016), clearly showing evolution not only in the average, but even more so on the spread, revealing very high EWs that simply are not seen at the peak of star formation history.

the much higher number density of very luminous sources. We also confirm that those additional sources are all X-ray sources, but we check that the vast majority are spectroscopically confirmed C III] and C IV emitters. We note that since *GALEX* data are also available, it is relatively easy to identify C III] and C IV emitters, as they will have Lyman-breaks at shorter wavelength than Lyα emitters, even if spectroscopic redshifts are not available.

Only spectroscopic follow-up can completely establish the exact shape of the bright end of the Lyα luminosity function (for the remaining 50 per cent of the sources spectroscopic redshifts are not currently available). We have already followed-up further two of the bright line emitters with XSHOOTER on the VLT in 2016 October without any Lyα pre-selection, confirming an N V$_{1239}$ emitter (with broad Lyα) at $z = 2.15$, and one Lyα emitter at $z = 2.2088$, in line with our expectations of relatively high contamination. These sources will be presented in a future paper, together with the rest of the ongoing follow-up on the VLT. Nevertheless, we can already conclude that it is crucial to remove contaminants, even for surveys in the bluest optical bands like ours. Our 'Lyα' luminosity function obtained by using all NB392 emitters can also be seen as a strong upper limit for the real Lyα luminosity function, as it already contains a significant number of confirmed contaminants, which become more and more significant at the highest luminosities. As our data allow us to derive contamination fractions per bin, we compute them and apply them to Konno et al. (2016), to derive a Lyα luminosity function which is fully comparable to ours. We show the results in Fig. 7. The CC to log (Φ) we derive are well described as a function of Lyα luminosity: CC $= -0.28\, L_{\rm Ly\alpha} + 11.732$ for $L_{\rm Ly\alpha} \approx 10^{42–44.5}$ erg s^{-1}. We note that if one fits the Lyα luminosity function with a Schechter function up to $L_{\rm Ly\alpha} \sim 10^{43}$ erg s^{-1} the contamination effect is still relatively small with $\log L^*_{\rm Ly\alpha}$ being overestimated by $\approx$0.15 dex and $\log \phi^*_{\rm Ly\alpha}$ being underestimated (as a consequence of the change in L^*) by $\approx$0.1 dex. However, contamination plays a major role for the highest luminosities and for determining the apparent power-law component of the Lyα luminosity function.

5.3 The EW distribution of Lyα emitters at $z = 2.23$ and implications for the Lyα luminosity function

As discussed in Section 5.2, the choice of Lyα rest-frame EW cut may have important effects in conclusions regarding the nature of Lyα emitters. Traditionally, due to the FWHM of typical narrow-band filters, and particularly due to the early difficulty in applying colour–colour and/or photometric redshift selections to differentiate between Lyα and other line emitters,[1] a relatively high EW cut was used. This assured that lower redshift emitters would be excluded. The typical value for this cut has been EW$_0 \sim 25$ Å.

As we are able to probe down to an Lyα rest-frame EW of 5 Å, we have the opportunity to investigate how complete samples with higher rest-frame EW cuts may be and what is the effect on e.g. the Lyα luminosity function. Fig. 9 shows the distribution of Lyα rest-frame EWs at $z = 2.23$. We find that the median EW$_0$ at $z = 2.23$

[1] This becomes more problematic for higher redshift Lyα surveys, as Lyα emitters become a progressively lower fraction of the full sample of emitters; see e.g. Matthee et al. (2014) or Matthee et al. (2015).

is $\approx$100 Å, with a tail at both higher rest-frame EWs (highest: 390 Å) and lower (lowest: 5.1 Å). If we were to apply a cut at $\mathrm{EW_0} > 25$ Å, we would still recover 89 per cent of our full sample of Lyα emitters. By imposing a cut of $\mathrm{EW_0} > 50$ Å, we would only recover 69 per cent of all Lyα emitters.

In Fig. 9, we also compare the rest-frame EW distribution of our Lyα emitters with Hα emitters at the same redshift (Sobral et al. 2014) and the EW distribution of Lyα emitters at higher redshift ($z = 5.7$; Santos et al. 2016). We find that Hα emitters at $z = 2.23$ show much higher EWs than Lyα-selected sources at the same redshift. Interestingly, if one reduces the Hα EWs by $\approx$60 per cent, the distribution becomes relatively similar to the one observed in Lyα, i.e. Lyα and Hα have a similar dispersion of EWs. This is not at all the case for the distribution of EWs for higher redshift Lyα emitters, selected over a similar range in luminosities from Santos et al. (2016). Lyα emitters at $z \sim 6$ present a much broader EW distribution, with a tail at very high EWs. These high EW Lyα emitters become much rarer at lower redshift.

By applying different EW cuts, we also study the effect of those on the Lyα luminosity function at $z = 2.23$. For all $\mathrm{EW_0}$ cuts, we repeat our Lyα selection, in order to eliminate interlopers, as described in Section 3.3.2. Also, for each new selection, as our EW cut changes, our completeness also changes, and thus we re-compute it and apply the appropriate corrections for each cut. This means that while a higher $\mathrm{EW_0}$ cut results in a lower completeness, our corrections can account for at least part of that. We show our results in Fig. 8, which shows the effect of varying the Lyα $\mathrm{EW_0}$.

We find that for Lyα-selected samples, a higher EW cut preferentially lowers the number densities at the bright end, eliminating the power-law component, and making the luminosity function (LF) look steeper. On the other hand, a simple EW cut, without filtering out the non-Lyα emitters from the sample, still leads to significant contamination at all luminosities, particularly at the bright end. We find that in order to eliminate such contaminants effectively one requires a relatively high $\mathrm{EW_0}$ of at least $>$50 Å, but that is far from ideal, as it will also eliminate a significant fraction of real luminous Lyα emitters, which we know are spectroscopically confirmed to be at $z = 2.23$.

6 THE LYα ESCAPE FRACTION AT $z = 2.23$

6.1 Lyα emitters at $z = 2.23$: the Hα view

The Hα stack of our Lyα emitters allows us to compute the typical SFR of our Lyα emitters. We use Kennicutt (1998) with a Chabrier initial mass function (Chabrier 2003), and correct Hα for extinction using Garn & Best (2010), following e.g. Sobral et al. (2014). Our results show that our sample of Lyα-selected sources has a median dust-corrected SFR of 7.7 ± 0.6 M$_\odot$ yr^{-1}. Such median SFR implies that our Lyα emitters are $\sim$0.1 SFR* star-forming galaxies at $z = 2.2$ (Sobral et al. 2014).

In Fig. 10, we show the Hα stack, a comparison to the rest-frame (Hα subtracted) R-band stack, and the Lyα stack of all our Lyα emitters. We find that Lyα is significantly more extended (diameter of about $\sim$40 kpc) than Hα by about a factor of 2. Our results are consistent with those presented in Matthee et al. (2016b) for a sub-set of Lyα–Hα emitters at $z = 2.23$, and reveal that Lyα emitters have ubiquitous extended Lyα emission (see also e.g. Momose et al. 2014; Matthee et al. 2016b; Wisotzki et al. 2016). When compared to Momose et al. (2014), we seem to find slightly larger Lyα extents, although our sample is dominated by brighter Lyα emitters than those in Momose et al. (2014), while our PSF is also larger than Momose et al. (2014). The combined effects (more luminous Lyα emitters in our sample and larger PSF) can likely explain the larger extents that we measure.

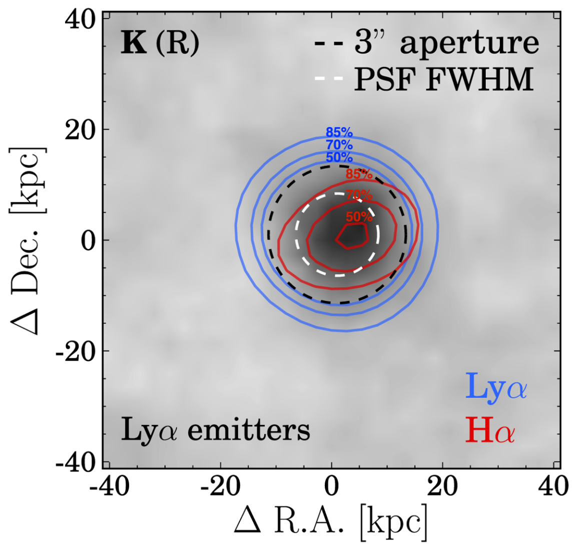

Figure 10. Stacked Hα and Lyα images of all our Lyα emitters. All bands are PSF matched and we show the common PSF in the image. We compare the stacked rest-frame R band (observed K band, Hα subtracted), tracing the older stellar population/stellar mass, with both Hα and Lyα emission from our sample of Lyα-selected emitters. Lyα and Hα contours show the 50, 70 and 85 per cent contours of the total flux. For a 3 arcsec diameter aperture, we recover 82 per cent of the total Hα flux (0.4×10^{-16} erg s^{-1}) but only 50 per cent of the total Lyα flux (2.2×10^{-16} erg s^{-1}). We thus find that while Hα is slightly more extended than the continuum emission, the Lyα emission extends to much larger radii. This is consistent with the results from Matthee et al. (2016b).

6.2 Lyα escape fraction and dependence on Lyα luminosity and $\mathrm{EW_0}$

Assuming case B recombination, we use the Hα stack (after applying all corrections; see Section 4.3) to measure an escape fraction of 37 ± 7 per cent for a 3 arcsec aperture. We also use larger apertures for both Lyα and Hα and find that the Lyα escape fraction increases with increasing aperture. We find this to be the case up to an aperture of 8 arcsec, when the Lyα escape fraction reaches an apparent plateau of 65 ± 20 per cent, consistent with Matthee et al. (2016b). Regardless of the aperture used, the values are significantly above the global average or the escape fraction for Hα selected/more typical star-forming galaxies, which is only a few per cent (see e.g. Hayes et al. 2010; Konno et al. 2016; Matthee et al. 2016b), as we will also show in Section 6.3. However, this is not surprising, as, by definition, Lyα emitters will have to have relatively high escape fractions, otherwise they would not be selected as such.

We then split our Lyα emitters according to their Lyα luminosity and $\mathrm{EW_0}$ (see Fig. 11). We find that the Lyα escape fraction increases with increasing $\mathrm{EW_0}$, with $f_{\rm esc}$ increasing from $\approx$18 per cent for $\mathrm{EW_0} \approx 40$ Å to $f_{\rm esc} \approx 70$ per cent for $\mathrm{EW_0} \approx 120$ Å. This is consistent with the younger/more star-bursting sources having higher Lyα escape fractions (see also Verhamme et al. 2016). We compare our results with measurements from the literature, including a sample of recently discovered LyC leakers at $z \sim 0.3$ (Izotov

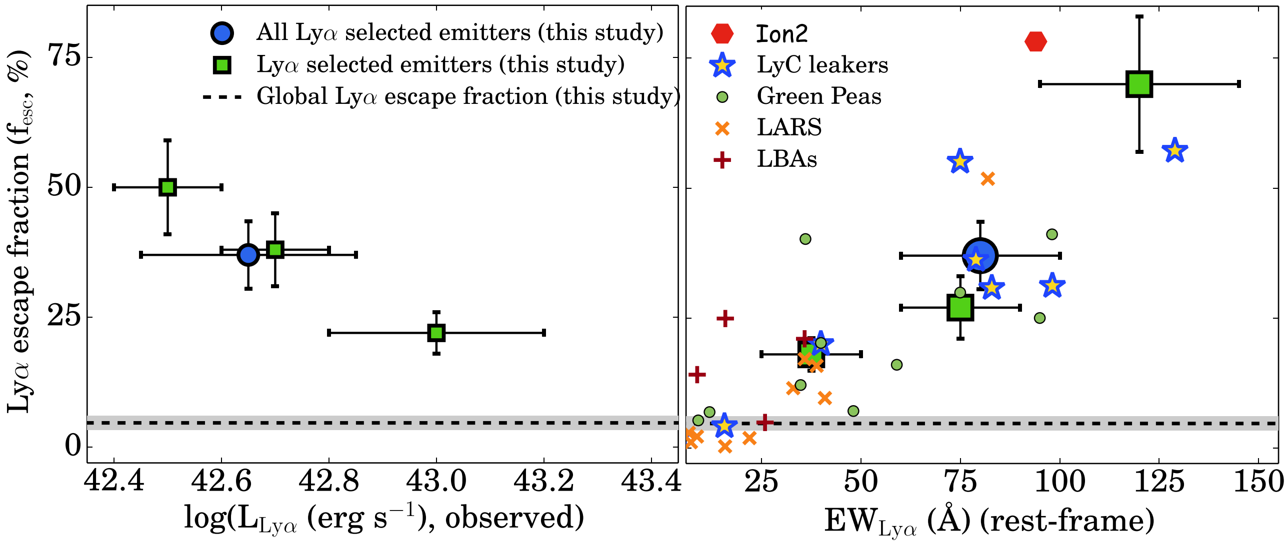

Figure 11. Left: the escape fraction (within ≈13 kpc) of Lyα emitters as a function of Lyα luminosity. The results show that more luminous Lyα emitters have lower escape fractions than those which are less luminous, but consistent with still having very high escape fractions even at the highest Lyα luminosities. Right: the escape fraction of Lyα photons increases as function of rest-frame Lyα EW. We also compare our results with similar measurements done for a range of Lyα-emitting galaxies mostly in the local Universe, and find that they all follow a similar relation to our $z = 2.2$ Lyα emitters. These include the recently discovered LyC leakers ($z \sim 0.3$; Izotov et al. 2016a,b; Verhamme et al. 2016), a Lyα–LyC leaker at $z = 3.2$, 'Ion2' (de Barros et al. 2016; Vanzella et al. 2016), green peas ($z \sim 0.3$; e.g. Cardamone et al. 2009; Henry et al. 2015; Yang et al. 2016), LBAs ($z \sim 0.2$; e.g. Heckman et al. 2005; Overzier et al. 2009) and the LARS ($z \sim 0.1$; e.g. Hayes et al. 2014; Östlin et al. 2014). The fact that our Lyα emitters follow the relation of confirmed LyC emitters could suggest that at least part of our Lyα emitters may be LyC leakers.

et al. 2016a,b; Verhamme et al. 2016), a Lyα–LyC leaker at $z = 3.2$, 'Ion2' (de Barros et al. 2016; Vanzella et al. 2016), and $z \sim 0.1$–0.3 sources such as: green peas (e.g. Cardamone et al. 2009; Henry et al. 2015; Yang et al. 2016), Lyman-break Analogues (LBAs; e.g. Heckman et al. 2005; Overzier et al. 2009) and the Lyman Alpha Reference Survey (LARS; e.g. Hayes et al. 2014; Östlin et al. 2014). Interestingly, we find that all these Lyα emitters follow a similar relation, with the Lyα escape fraction rising with increasing Lyα rest-frame EW, even though they are found at very different redshifts and have been pre-selected through different methods. It is particularly interesting that green peas and the confirmed LyC emitters at low redshift, and 'Ion2', a confirmed LyC leaker at $z = 3.2$ populate the highest escape fraction and highest EWs that we find in our sample. The results suggest that our high EW Lyα-selected sources at $z \sim 2$ may be very good LyC leaker candidates.

Naïvely, f_{esc} could be expected to increase with Lyα luminosity. However, as Fig. 11 shows, we find that f_{esc} decreases with increasing Lyα luminosity. For our faintest luminosity bin, $L_{Ly\alpha} \approx 10^{42.5}$ erg s^{-1}, we measure $f_{esc} = 50 \pm 9$ per cent, while we only measure $f_{esc} = 22 \pm 4$ per cent for the most luminous bin, $L_{Ly\alpha} \approx 10^{43.0}$ erg s^{-1}. When interpreted together with results from Section 6.3, it is expected that f_{esc} will drop again for very low Lyα luminosities. We discuss this in more detail in Section 7.

6.3 The global Ly α escape fraction at $z = 2.23$

Here, we investigate the global escape fraction of Lyα photons (with a fixed 3 arcsec diameter aperture) at the peak epoch of the star formation history of the Universe. We focus on the global escape fraction (from the integral of the Lyα and Hα luminosity functions) and use the extinction corrected Hα luminosity function presented by Sobral et al. (2013).

The Schechter component of our fit to the Lyα luminosity function yields an integrated luminosity density (full integral) of 1.1×10^{40} erg s^{-1} Mpc^{-3}. The additional power-law component adds a further 1.1×10^{39} erg s^{-1} Mpc^{-3}, or ∼10 per cent of the Schechter contribution. However, it should be noted that if one integrates down to e.g. $L_{Ly\alpha} > 10^{41.6}$ erg s^{-1}, the Schechter component becomes only 0.4×10^{40} erg s^{-1} Mpc^{-3}, and thus the power-law component becomes more important for shallower Lyα surveys.

By integrating our Lyα luminosity function at $z = 2.23$, assuming case B recombination, and directly comparing with the equivalent integral of the extinction-corrected Hα luminosity function, we find that, on average, within the same apertures used for Hα and Lyα (corresponding to roughly to a 13 kpc radius), only 5.1 ± 0.2 per cent of Lyα photons escape. This is in very good agreement with the measurement from Hayes et al. (2010) of 5 ± 4 per cent, but our result greatly reduces the errors due to a much larger volume and significantly larger samples. More recently, Matthee et al. (2016b) studied an Hα-selected sample, finding that, down to the detection limit of the sample, the Lyα escape fraction is 1.6 ± 0.5 per cent. However, those authors show that the escape fraction strongly anticorrelates with Hα flux/SFR, with the low Hα flux and low SFR galaxies having the highest Lyα escape fractions. Thus, the results in Matthee et al. (2016b) are in very good agreement with our global escape fraction of 5.1 ± 0.2 per cent, particularly due to the contribution of much lower SFR sources to the global measurement.

The results presented by Matthee et al. (2016b) already hint that Lyα escape fractions will strongly depend on e.g. the Hα luminosity limit of a survey (and also depend strongly on the aperture used). Thus, while we find a typical escape fraction of 5.1 ± 0.2 per cent by integrating both the Hα and the Lyα luminosity functions, we also study the effect of integrating down to different luminosity limits. Our full results are presented in Table 4.

Table 4. Lyα (observed) and Hα (extinction corrected) luminosity densities for different integration limits and different assumptions, including integrating down to the same limits, but also integrating down to limits scaled by a factor of 8.7 (labelled 'B'). For each set of luminosity densities, we assume case B recombination and compute the escape fraction of Lyα photons (a factor of 8.7). All Lyα luminosity densities have been computed taking into account the power-law component. To obtain the Schechter luminosity density only, one simply has to remove the fixed contribution of 1.1×10^{39} erg s^{-1} Mpc^{-3}. Note that all these measurements are based on 3 arcsec apertures; for Lyα emitters we find that those may only recover about 50 per cent of the Lyα flux, but recover around 80 per cent of the Hα, implying a potential aperture correction of 1.64.

Integration limit	$\log\rho_{L_{\rm Ly\alpha}}$ erg s^{-1} Mpc^{-3}	$\log\rho_{L_{\rm H\alpha}}$ erg s^{-1} Mpc^{-3}	Lyα $f_{\rm esc}$ (%)
$10^{41.0}$	39.87 ± 0.02	40.34 ± 0.02	3.9 ± 0.3
$10^{41.6}$	39.74 ± 0.02	40.25 ± 0.02	3.5 ± 0.3
$10^{42.0}$	39.59 ± 0.02	40.15 ± 0.02	3.2 ± 0.3
$10^{41.0}$ (B)	39.97 ± 0.02	40.34 ± 0.02	4.9 ± 0.4
$10^{41.6}$ (B)	39.91 ± 0.02	40.25 ± 0.02	5.3 ± 0.4
$10^{42.0}$ (B)	39.86 ± 0.02	40.15 ± 0.02	5.9 ± 0.5
0.01 L^*	39.92 ± 0.02	40.35 ± 0.02	4.3 ± 0.4
0.1 L^*	39.74 ± 0.01	40.18 ± 0.02	4.1 ± 0.3
0.2 L^*	39.64 ± 0.01	40.08 ± 0.02	4.2 ± 0.3
L^*	39.27 ± 0.02	39.51 ± 0.02	6.5 ± 0.4
Full	40.08 ± 0.02	40.43 ± 0.02	$\mathbf{5.1 \pm 0.2}$

Furthermore, as shown in Fig. 10, we find that at a fixed 3 arcsec we recover a much larger fraction of the total Hα flux (82 per cent; consistent with e.g. Sobral et al. 2014) than the total Lyα flux (50 per cent). If we apply these results to correct the integral of the Hα and Lyα luminosity functions, we find that the total (aperture corrected) average Lyα escape fraction would be 1.64 times larger, or 8.4 ± 0.3 per cent. This means that, potentially, a further 3.3 per cent of Lyα photons still escape, but at larger radii than those that our 3 arcsec diameter apertures capture.

Of particular importance is the fact that if one does not integrate both e.g. Hα (or UV) and Lyα fully, one needs to be careful about the limit one integrates down to. It is very clear from all observational work that Lyα luminosities show significant scatter and a non-linear behaviour as a function of either UV or Hα (e.g. Matthee et al. 2016b), due to significant changes in escape fraction as function of various properties. This is further highlighted by our results on the escape fraction by stacking in Hα (only possible with our data set). This shows that the escape fraction changes significantly with Lyα luminosity, and that there certainly is not a 1:1 correlation between Hα and Lyα. Thus, the results of integrating down to a specific luminosity are not easily interpreted. For example, a 0.1 L^* Hα emitter is not necessarily a 0.1 L^* Lyα emitter and vice versa. This means that integrating down to a different L^* will lead to a different escape fraction. We illustrate this by obtaining escape fractions based on integrations of the Hα and Lyα luminosity functions down to different limits in Table 4.

7 CONCLUSIONS

We presented the first results from the CALYMHA pilot survey conducted at the INT over the COSMOS and UDS fields. We used a custom-built Lyα narrow-band filter, NB392 ($\lambda_c = 3918$ Å, $\Delta\lambda = 52$ Å), on the WFC, to survey large extragalactic fields at $z = 2.23$. Our NB392 filter ($\lambda_c = 3918$ Å, $\Delta\lambda = 52$ Å) has been designed to provide a matched volume coverage to the $z = 2.23$ HiZELS survey conducted with UKIRT (Sobral et al. 2013). CALYMHA currently reaches a line flux limit of $\sim 4 \times 10^{-17}$ erg s^{-1} cm^{-2}, and a Lyα luminosity limit of $\sim 10^{42.3}$ erg s^{-1} (3σ). Our main results are as follows.

(i) We obtained a sample of 440 line emitters in COSMOS and UDS. Among them, and apart from Lyα emitters, we find a significant population of spectroscopically confirmed [O II], He II, C III] and C IV line emitters. C IV emitters at $z \sim 1.5$ represent $\sim$25 per cent of line emitters with an available spectroscopic redshift. We show how important it is for Lyα surveys to remove contaminants, especially C III] and C IV (which many have incorrectly assumed to be unimportant). Removing those contaminants is essential to robustly determine the bright end of the Lyα luminosity function.

(ii) We use spectroscopic and photometric redshifts, together with colour–colour selections, to select a clean and complete sample of 188 Lyα emitters over a volume of 7.3×10^5 Mpc^3.

(iii) We show that the Lyα luminosity function is significantly overestimated if all line emitters are used, with a simple equivalent cut. Such simple selections (single EW cut) are particularly problematic at higher fluxes, where contaminants become more and more important, particularly spectroscopically confirmed C III] and C IV emitters (AGN), which can have $\mathrm{EW}_0 > 25$ Å.

(iv) The Lyα luminosity function at $z = 2.23$ is very well described by a Schechter function up to $L_{\rm Ly\alpha} \approx 10^{43}$ erg s^{-1} with $L^* = 10^{42.59^{+0.16}_{-0.08}}$ erg s^{-1}, $\phi^* = 10^{-3.09^{+0.14}_{-0.34}}$ Mpc^{-3} and $\alpha = -1.75 \pm 0.25$.

(v) Beyond $L_{\rm Ly\alpha} \approx 10^{43}$ erg s^{-1}, the Lyα luminosity function becomes power-law like, similarly to what has been found in Konno et al. (2016) at $z = 2.2$, due to the prevalence of bright X-ray AGN with similar X-ray and Lyα luminosities. However our normalization of the power-law component is significantly below that of Konno et al. (2016). We note that our results are based on a sample, which is $\sim$50 per cent spectroscopically complete and cleaned of contaminants.

(vi) We show that the bright end of the Lyα luminosity function depends strongly on the choice of EW cut applied, as the sample of bright Lyα emitters becomes increasingly incomplete as a function of EW cut. Selections with a very high EW cut (usually motivated to eliminate contaminants) lose the power-law component and fail to select real, spectroscopically confirmed Lyα emitters.

(vii) By stacking the Hα narrow-band images of our Lyα emitters in Hα, we find that they have a median dust corrected Hα SFR of 7.7 ± 0.6 M$_\odot$ yr^{-1} ($\sim$0.1 SFR* at $z = 2.2$), and have an escape fraction (Lyα photons) of 37 ± 7 per cent. Lyα emission from our stack of Lyα emitters extends ($\approx$40 kpc) by about 2 times that of the Hα emission, in very good agreement with Matthee et al. (2016b).

(viii) We find that the Lyα escape fraction of Lyα emitters at $z = 2.23$ drops with increasing Lyα luminosity, and increases with increasing Lyα rest-frame EW. This may be due to sources with high EWs being generally younger, less dusty and less massive, favouring high escape fractions. Sources with the highest Lyα luminosities are dominated by X-ray-detected AGN.

(ix) By directly comparing our Lyα and Hα luminosity functions, which are not affected by cosmic variance and are obtained over the same multiple large volumes, we find that the global escape fraction of Lyα from star-forming galaxies at $z = 2.23$ is 5.1 ± 0.2 per cent. We also show how important the choice of integration limits is, given that the Lyα escape fraction varies significantly both with Lyα luminosity, as shown in this paper, but also as a function of Hα luminosity (Matthee et al. 2016b) in a non-linear way.

Our results imply that 94.9 ± 0.2 per cent of the total Lyα luminosity density produced at the peak of the star formation history ($z \sim 2$) does not escape the host galaxies within a radius of ∼13 kpc (3 arcsec diameter aperture). Integrating the luminosity functions down to observed values yields a lower escape fraction, in agreement with e.g. Matthee et al. (2016b) and Konno et al. (2016). Also, we show that for Lyα-selected samples, the escape fraction is, not surprisingly, significantly above the cosmic average we measure (5.1 ± 0.2 per cent), and around 37 per cent for a 3 arcsec aperture. Interestingly, and even though this already corresponds to a quite high escape fraction, it is only a lower limit as far as the total escape fraction (at any radii) is concerned, as we clearly see that Lyα extends beyond the Hα emission by a factor of ∼2 and the radius usually used to measure emission line properties (see also Wisotzki et al. 2016; Drake et al. 2016). This means that an extra 3.3 ± 0.3 per cent of Lyα photons likely still escape, but at larger radii, potentially adding up to a total escape fraction at any radii of ∼8 per cent, although this is highly uncertain. Nevertheless, significant progress can be further achieved with new instruments such as MUSE (e.g. Wisotzki et al. 2016; Borisova et al. 2016).

Our results provide important empirical measurements that are useful to interpret observations at higher redshift. Significantly deeper Lyα–Hα observations, and observations spread over more fields will allow for further significant progress. Moreover, once *JWST* is launched, it will be possible to directly measure Hα from both UV and Lyα-selected sources, and thus some of the results from our survey can then be tested at higher redshift.

ACKNOWLEDGEMENTS

We thank the reviewer for his/her helpful comments and suggestions that have greatly improved this work. DS and JM acknowledge financial support from the Netherlands Organisation for Scientific research (NWO) through a Veni fellowship. DS also acknowledges funding from FCT through an FCT Investigator Starting Grant and Start-up Grant (IF/01154/2012/CP0189/CT0010). PNB is grateful for support from the UK STFC via grant ST/M001229/1. IRS acknowledges support from STFC (ST/L00075X/1), the ERC Advanced Investigator programme DUSTYGAL 321334 and a Royal Society/Wolfson merit award. We thank Matthew Hayes, Ryan Trainor, Kimihiko Nakajima and Anne Verhamme for many helpful discussions and Ana Sobral, Carolina Duarte and Miguel Domingos for taking part in observations with the NB392 filter. We also thank Sergio Santos for helpful comments. This research is based on observations obtained on the Isaac Newton Telescope (INT), programs: I13AN002, I14AN002, 088-INT7/14A, I14BN006, 118-INT13/14B & I15AN008. The authors acknowledge the award of time from programmes: I13AN002, I14AN002, 088-INT7/14A, I14BN006, 118-INT13/14B, I15AN008 on the INT. INT is operated on the island of La Palma by the Isaac Newton Group in the Spanish Observatorio del Roque de los Muchachos of the Instituto de Astrofisica de Canarias. Based on observations made with ESO Telescopes at the La Silla Paranal Observatory under programme ID 098.A-0819. We have benefited greatly from the publicly available programming language PYTHON, including the NUMPY, MATPLOTLIB, PYFITS, SCIPY and ASTROPY packages, the astronomical imaging tools SEXTRACTOR, SWARP (Bertin & Arnouts 1996; Bertin 2010), SCAMP (Bertin 2006) and TOPCAT (Taylor 2005). Dedicated to the memory of M. L. Nicolau and M. C. Serrano.

REFERENCES

Atek H., Kunth D., Hayes M., Östlin G., Mas-Hesse J. M., 2008, A&A, 488, 491
Atek H., Kunth D., Schaerer D., Hayes M., Deharveng J. M., Östlin G., Mas-Hesse J. M., 2009, A&A, 506, L1
Atek H., Kunth D., Schaerer D., Mas-Hesse J. M., Hayes M., Östlin G., Kneib J.-P., 2014, A&A, 561, A89
Bacon R. et al., 2015, A&A, 575, A75
Barger A. J., Cowie L. L., Wold I. G. B., 2012, ApJ, 749, 106
Bertin E., 2006, in Gabriel C., Arviset C., Ponz D., Enrique S., eds, ASP Conf. Ser. Vol. 351, Astronomical Data Analysis Software and Systems XV. Astron. Soc. Pac., San Francisco, p. 112
Bertin E., 2010, Astrophysics Source Code Library, ascl:1010.068
Bertin E., Arnouts S., 1996, A&AS, 117, 393
Blanc G. A. et al., 2011, ApJ, 736, 31
Bongiovanni A. et al., 2010, A&A, 519, L4
Borisova E. et al., 2016, ApJ, 831, 39
Bouwens R. J. et al., 2015, ApJ, 803, 34
Bunker A. J., Warren S. J., Hewett P. C., Clements D. L., 1995, MNRAS, 273, 513
Capak P. et al., 2007, ApJS, 172, 99
Cardamone C. et al., 2009, MNRAS, 399, 1191
Cassata P. et al., 2011, A&A, 525, A143
Chabrier G., 2003, PASP, 115, 763
Chapman S. C., Blain A. W., Smail I., Ivison R. J., 2005, ApJ, 622, 772
Ciardullo R. et al., 2012, ApJ, 744, 110
Ciardullo R. et al., 2014, ApJ, 796, 64
Cirasuolo M., McLure R. J., Dunlop J. S., Almaini O., Foucaud S., Simpson C., 2010, MNRAS, 401, 1166
Civano F. et al., 2012, ApJS, 201, 30
Civano F. et al., 2016, ApJ, 819, 62
Cowie L. L., Barger A. J., Hu E. M., 2010, ApJ, 711, 928
Daddi E., Cimatti A., Renzini A., Fontana A., Mignoli M., Pozzetti L., Tozzi P., Zamorani G., 2004, ApJ, 617, 746
de Barros S. et al., 2016, A&A, 585, A51
Dijkstra M., 2014, PASA, 31, 40
Dijkstra M., Lidz A., Wyithe J. S. B., 2007, MNRAS, 377, 1175
Dijkstra M., Gronke M., Venkatesan A., 2016, ApJ, 828, 71
Drake A. B. et al., 2016, preprint (arXiv:1609.02920)
Erb D. K. et al., 2014, ApJ, 795, 33
Erb D. K., Pettini M., Steidel C. C., Strom A. L., Rudie G. C., Trainor R. F., Shapley A. E., Reddy N. A., 2016, ApJ, 830, 52
Garel T., Blaizot J., Guiderdoni B., Michel-Dansac L., Hayes M., Verhamme A., 2015, MNRAS, 450, 1279
Garn T., Best P. N., 2010, MNRAS, 409, 421
Gawiser E. et al., 2007, ApJ, 671, 278
Geach J. E., Simpson C., Rawlings S., Read A. M., Watson M., 2007, MNRAS, 381, 1369
Giavalisco M., 2002, ARA&A, 40, 579
Gronke M., Dijkstra M., 2016, ApJ, 826, 14
Gronke M., Bull P., Dijkstra M., 2015, ApJ, 812, 123
Gronwall C. et al., 2007, ApJ, 667, 79
Hashimoto T., Ouchi M., Shimasaku K., Ono Y., Nakajima K., Rauch M., Lee J., Okamura S., 2013, ApJ, 765, 70
Hathi N. P. et al., 2016, A&A, 588, A26
Hayes M., 2015, PASA, 32, e027
Hayes M. et al., 2010, Nature, 464, 562
Hayes M., Schaerer D., Östlin G., Mas-Hesse J. M., Atek H., Kunth D., 2011, ApJ, 730, 8
Hayes M. et al., 2014, ApJ, 782, 6
Heckman T. M. et al., 2005, ApJ, 619, L35
Henry A., Scarlata C., Martin C. L., Erb D., 2015, ApJ, 809, 19
Hernquist L., Katz N., Weinberg D. H., Miralda-Escudé J., 1996, ApJ, 457, L51
Ibar E. et al., 2013, MNRAS, 434, 3218
Ilbert O. et al., 2009, ApJ, 690, 1236

Izotov Y. I., Schaerer D., Thuan T. X., Worseck G., Guseva N. G., Orlitová I., Verhamme A., 2016a, MNRAS, 461, 3683
Izotov Y. I., Orlitová I., Schaerer D., Thuan T. X., Verhamme A., Guseva N. G., Worseck G., 2016b, Nature, 529, 178
Karim A. et al., 2011, ApJ, 730, 61
Karman W. et al., 2015, A&A, 574, A11
Kashikawa N. et al., 2006, ApJ, 648, 7
Kashikawa N. et al., 2012, ApJ, 761, 85
Kennicutt R. C., Jr1998, ARAA, 36, 189
Khostovan A. A., Sobral D., Mobasher B., Best P. N., Smail I., Stott J. P., Hemmati S., Nayyeri H., 2015, MNRAS, 452, 3948
Khostovan A. A., Sobral D., Mobasher B., Smail I., Darvish B., Nayyeri H., Hemmati S., Stott J. P., 2016, MNRAS, 463, 2363
Konno A., Ouchi M., Nakajima K., Duval F., Kusakabe H., Ono Y., Shimasaku K., 2016, ApJ, 823, 20
Lawrence A. et al., 2007, MNRAS, 379, 1599
Le Delliou M., Lacey C. G., Baugh C. M., Morris S. L., 2006, MNRAS, 365, 712
Lilly S. J., Le Fevre O., Hammer F., Crampton D., 1996, ApJ, 460, L1
Lilly S. J. et al., 2009, ApJS, 184, 218
McCracken H. J. et al., 2012, A&A, 544, A156
Malhotra S., Rhoads J. E., 2004, ApJ, 617, L5
Matthee J. J. A. et al., 2014, MNRAS, 440, 2375
Matthee J., Sobral D., Santos S., Röttgering H., Darvish B., Mobasher B., 2015, MNRAS, 451, 400
Matthee J., Sobral D., Best P., Khostovan A. A., Oteo I., Bouwens R., Röttgering H., 2016a, preprint (arXiv:1605.08782)
Matthee J., Sobral D., Oteo I., Best P., Smail I., Röttgering H., Paulino-Afonso A., 2016b, MNRAS, 458, 449
Momose R. et al., 2014, MNRAS, 442, 110
Murayama T. et al., 2007, ApJS, 172, 523
Muzzin A. et al., 2013, ApJS, 206, 8
Nagamine K., Ouchi M., Springel V., Hernquist L., 2010, PASJ, 62, 1455
Nakajima K. et al., 2012, ApJ, 745, 12
Nakajima K., Ellis R. S., Iwata I., Inoue A., Kusakabe H., Ouchi M., Robertson B., 2016, ApJL, preprint (arXiv:1608.08222)
Nilsson K. K., Tapken C., Møller P., Freudling W., Fynbo J. P. U., Meisenheimer K., Laursen P., Östlin G., 2009, A&A, 498, 13
Oesch P. A. et al., 2015, ApJ, 804, L30
Ono Y. et al., 2010a, MNRAS, 402, 1580
Ono Y., Ouchi M., Shimasaku K., Dunlop J., Farrah D., McLure R., Okamura S., 2010b, ApJ, 724, 1524
Ono Y. et al., 2012, ApJ, 744, 83
Östlin G. et al., 2014, ApJ, 797, 11
Oteo I. et al., 2012a, A&A, 541, A65
Oteo I. et al., 2012b, ApJ, 751, 139
Oteo I., Sobral D., Ivison R. J., Smail I., Best P. N., Cepa J., Pérez-García A. M., 2015, MNRAS, 452, 2018
Ouchi M. et al., 2008, ApJs, 176, 301
Ouchi M. et al., 2010, ApJ, 723, 869
Overzier R. A. et al., 2009, ApJ, 706, 203
Partridge R. B., Peebles P. J. E., 1967, ApJ, 147, 868
Pritchet C. J., 1994, PASP, 106, 1052
Rauch M. et al., 2008, ApJ, 681, 856
Saintonge A. et al., 2011, MNRAS, 415, 32
Sandberg A., Guaita L., Östlin G., Hayes M., Kiaeerad F., 2015, A&A, 580, A91
Santos S., Sobral D., Matthee J., 2016, MNRAS, 463, 1678
Sargent W. L. W., Young P. J., Boksenberg A., Tytler D., 1980, ApJS, 42, 41
Simpson C. et al., 2006, MNRAS, 372, 741
Smail I., Sharp R., Swinbank A. M., Akiyama M., Ueda Y., Foucaud S., Almaini O., Croom S., 2008, MNRAS, 389, 407
Smit R., Bouwens R. J., Franx M., Illingworth G. D., Labbé I., Oesch P. A., van Dokkum P. G., 2012, ApJ, 756, 14
Sobral D., Best P. N., Matsuda Y., Smail I., Geach J. E., Cirasuolo M., 2012, MNRAS, 420, 1926
Sobral D., Smail I., Best P. N., Geach J. E., Matsuda Y., Stott J. P., Cirasuolo M., Kurk J., 2013, MNRAS, 428, 1128
Sobral D., Best P. N., Smail I., Mobasher B., Stott J., Nisbet D., 2014, MNRAS, 437, 3516
Sobral D. et al., 2015a, MNRAS, 451, 2303
Sobral D., Matthee J., Darvish B., Schaerer D., Mobasher B., Röttgering H. J. A., Santos S., Hemmati S., 2015b, ApJ, 808, 139
Sobral D., Kohn S. A., Best P. N., Smail I., Harrison C. M., Stott J., Calhau J., Matthee J., 2016, MNRAS, 457, 1739
Song M. et al., 2014, ApJ, 791, 3
Stark D. P., Schenker M. A., Ellis R., Robertson B., McLure R., Dunlop J., 2013, ApJ, 763, 129
Steidel C. C., Giavalisco M., Pettini M., Dickinson M., Adelberger K. L., 1996, ApJ, 462, L17
Steidel C. C., Erb D. K., Shapley A. E., Pettini M., Reddy N., Bogosavljević M., Rudie G. C., Rakic O., 2010, ApJ, 717, 289
Stiavelli M., Scarlata C., Panagia N., Treu T., Bertin G., Bertola F., 2001, ApJ, 561, L37
Stott J. P. et al., 2016, MNRAS, 457, 1888
Stroe A., Sobral D., 2015, MNRAS, 453, 242
Stroe A., Sobral D., Röttgering H. J. A., van Weeren R. J., 2014, MNRAS, 438, 1377
Swinbank A. M. et al., 2015, MNRAS, 449, 1298
Tacconi L. J. et al., 2010, Nature, 463, 781
Taylor M. B., 2005, in Shopbell P., Britton M., Ebert R., eds, ASP Conf. Ser. Vol. 347, Astronomical Data Analysis Software and Systems XIV. Astron. Soc. Pac., San Francisco, p. 29
Trainor R. F., Steidel C. C., Strom A. L., Rudie G. C., 2015, ApJ, 809, 89
Trainor R. F., Strom A. L., Steidel C. C., Rudie G. C., 2016, ApJ, 832, 171
van Breukelen C. et al., 2007, MNRAS, 382, 971
Vanzella E. et al., 2016, ApJ, 825, 41
Vasei K. et al., 2016, preprint (arXiv:1603.02309)
Verhamme A., Schaerer D., Maselli A., 2006, A&A, 460, 397
Verhamme A., Schaerer D., Atek H., Tapken C., 2008, A&A, 491, 89
Verhamme A., Orlitová I., Schaerer D., Hayes M., 2015, A&A, 578, A7
Verhamme A., Orlitova I., Schaerer D., Izotov Y., Worseck G., Thuan T. X., Guseva N., 2016, A&A, preprint (arXiv:1609.03477)
Wardlow J. L. et al., 2014, ApJ, 787, 9
Wisotzki L. et al., 2016, A&A, 587, A98
Wold I. G. B., Barger A. J., Cowie L. L., 2014, ApJ, 783, 119
Yamada T. et al., 2005, ApJ, 634, 861
Yang H., Malhotra S., Gronke M., Rhoads J. E., Dijkstra M., Jaskot A., Zheng Z., Wang J., 2016, ApJ, 820, 130
Zitrin A. et al., 2015, ApJ, 810, L12

SUPPORTING INFORMATION

Supplementary data are available at *MNRAS* online.

Table A2. The first 9 entries from the catalogue of 440 candidate line emitters selected in COSMOS and UDS.

Please note: Oxford University Press is not responsible for the content or functionality of any supporting materials supplied by the authors. Any queries (other than missing material) should be directed to the corresponding author for the article.

APPENDIX A: CATALOGUES OF LINE EMITTERS

Table A2 presents example entries of the full catalogue of 440 line emitters, and a flag for sources selected as Lyα emitters. The full catalogue is available on the online version of the paper.

Table A1. The $z = 2.23$ Lyα luminosity function. We present both observed/raw number densities and number densities corrected taken into account incompleteness and the filter profile corrections.

log $L_{Ly\alpha}$	ϕ obs (Mpc^{-3})	ϕ corr (Mpc^{-3})	Volume (10^5 Mpc^3)
42.30 ± 0.125	-2.74 ± 0.10	-2.76 ± 0.11	0.539
42.55 ± 0.125	-3.06 ± 0.04	-3.11 ± 0.05	5.208
42.80 ± 0.125	-3.53 ± 0.06	-3.60 ± 0.07	7.123
43.05 ± 0.125	-4.32 ± 0.18	-4.40 ± 0.21	7.330
43.30 ± 0.125	-4.54 ± 0.25	-4.62 ± 0.30	7.330
43.55 ± 0.125	-5.07 ± 0.70	-5.15 ± 1.88	7.330

Table A2. The first nine entries from the catalogue of 440 candidate line emitters selected in COSMOS and UDS. The full catalogue is available online.

ID	RA (J2000)	Dec. (J2000)	NB392 (AB)	u (AB)	log Flux (erg s^{-1} cm^{-2})	EW_{obs} (Å)	Σ	Lyα selec.
CALYMHA-S16-1	10 02 42.916	+02 12 52.93	23.6	25.1	−15.9	248	3.1	No
CALYMHA-S16-2	10 02 42.318	+02 35 29.47	23.3	24.5	−15.9	121	3.9	Yes
CALYMHA-S16-3	10 02 39.342	+02 26 10.08	22.9	23.6	−15.8	55	3.3	No
CALYMHA-S16-4	10 02 38.841	+02 35 58.76	23.7	25.2	−15.9	246	3.4	No
CALYMHA-S16-5	10 02 37.020	+02 40 29.08	23.2	24.2	−15.9	95	4.0	No
CALYMHA-S16-6	10 02 36.829	+02 39 47.33	23.8	25.6	−16.0	375	3.1	Yes
CALYMHA-S16-7	10 02 36.770	+02 32 25.79	23.3	24.8	−15.8	212	4.6	Yes
CALYMHA-S16-8	10 02 35.458	+02 17 57.62	23.2	24.3	−15.8	113	3.5	Yes
CALYMHA-S16-9	10 02 35.106	+02 32 23.91	23.6	25.5	−15.9	377	3.6	Yes

This paper has been typeset from a TEX/LATEX file prepared by the author.